Modelling gaseous non-reactive flow in a Lean Direct Injection (LDI) Gas Turbine Combustor through an advanced mesh control strategy

Payri, R., Novella, R., Carreres, M. (*), Belmar-Gil, M.

CMT-Motores Térmicos, Universitat Politècnica de València

Camino de Vera s/n, E-46022 Spain

(*) Corresponding author:

Dr. Marcos Carreres, marcarta@mot.upv.es

CMT-Motores Térmicos, Universitat Politècnica de València

Camino de Vera s/n, E-46022 Spain

Telephone: +34 963 876 555

ABSTRACT

Fuel efficiency improvement and harmful emissions reduction are the main motivations for the development of gas turbine combustors. Numerical CFD simulations of these devices are usually computationally expensive since they imply a multi-scale problem. In this work, gaseous non-reactive U-RANS and LES simulations of a gaseous-fueled radial-swirled lean-direct injection (LDI) combustor have been carried out through CONVERGE™ CFD code by solving the complete inlet flow path through the swirl vanes and the combustor. The geometry considered is the gaseous configuration of the CORIA LDI combustor, for which detailed measurements are available. The emphasis of the work is placed on the demonstration of the CONVERGE™ applicability to the multi-scale Gas Turbine engines field and the determination of an optimal mesh strategy through several grid control tools (i.e., local refinement, adaptive mesh refinement) allowing the exploitation of its automatic mesh generation against traditional fixed mesh approaches. For this purpose, the Normalized Mean Square Error (NMSE) has been adopted to quantify the accuracy of turbulent numerical statistics regarding the agreement with the experimental database. Furthermore, the focus of the work is to study the behavior when coupling several LES sub-grid scale models (i.e., Smagorinsky, Dynamic Smagorinsky and Dynamic Structure) with the adaptive mesh refinement algorithm through the evaluation of its specific performances and predictive capabilities in resolving the spatial-temporal scales and the intrinsically unsteady flow structures generated within the combustor. This investigation on the main non-reacting swirling flow characteristics inside the combustor provides a suitable background for further studies on combustion instability mechanisms.

Payri, R., Novella, R., Carreres, M., Belmar-Gil, M, "Modeling gaseous non-reactive flow in a lean direct injection gas turbine combustor through an advanced mesh control strategy", Proceedings of the Institution of Mechanical Engineers, Part G: Journal of Aerospace Engineering 234(11):1788-1810, 2020 (author version).

doi: 10.1177/0954410020919619

KEYWORDS

Gas turbine combustor, Turbulent swirling flow, U-RANS, Large Eddy Simulation, Adaptive Mesh Refinement, Non-reactive flow, CONVERGE

LIST OF NOTATION

dx_k cell length in the three directions

f_{PVC} precession frecuency of the central vortex

k turbulent kinetic energy

R_i mean radius of the convergent inlet

R_{ext} outer radius of injection

S_W swirl number

$u_i^{'}$ turbulent fluctuation velocity

u_z axial velocity component

u_θ tangential velocity component

$u_{\theta,i}$ mean tangential velocity component in the inlet plane of the combustion chamber

y^+ non-dimensional distance to the wall

IQ_k index of quality of a LES simulation based on the resolved turbulent energy

IQ_v index of quality of a LES simulation based on the viscosity

GREEK SYMBOLS

ϕ swirl vane angle

ϕ_N numerical variable predicted by the CFD code

ϕ_E experimental variable measured in the test rig

Δt time step

τ_{PVC} precession period of the central vortex

τ_{rot} rotation time scale associated with the Vortex Breakdown Bubble

ABBREVIATIONS

AMR Adaptive Mesh Refinement

CFL Courant–Friedrichs–Lewy number

CPU Central Processing Unit

CRZ Corner Recirculation Zone

Payri, R., Novella, R., Carreres, M., Belmar-Gil, M, “Modeling gaseous non-reactive flow in a lean direct injection gas turbine combustor through an advanced mesh control strategy”, Proceedings of the Institution of Mechanical Engineers, Part G: Journal of Aerospace Engineering 234(11):1788-1810, 2020 (author version).

doi: 10.1177/0954410020919619

CTRZ Central Toroidal Recirculation Zone

DNS Direct Numerical Simulation

FE Fixed Embedding

LDI Lean Direct Injection

LDV Laser-Doppler Velocimetry

LES Large Eddy Simulation

LIF Laser Induced Fluorescence

LRR Launder-Reece-Rodi

NMSE Normalized Mean Square Error

NOx Nitrogen oxides

PDA Phase Doppler Anemometry

PVC Precessing Vortex Core

PISO Pressure Implicit with Splitting of Operators

RNG Renormalization Group

RMS Root Mean Square

RQL Rich Burn – Quick Mix – Lean Burn

RSM Reynolds Stress Models

SGS Sub-Grid Scales

SWJ Swirled Jet

U-RANS Unsteady Reynolds-Averaged Navier Stokes

VBB Vortex Breakdown Bubble

1. INTRODUCTION

The main challenge of the gas turbine aero-engines industry in the 21st century is to increase the efficiency of the cycle by keeping the levels of polluting emissions below the strict limits established by the regulatory organizations.[1] To this end, many high combustion efficiency and low emission combustor designs have been proposed. Among them, one specific concept, Lean Direct Injection (LDI), has been of particular focus due to its potential for excellent performance in terms of emissions at high-temperature and high-pressure conditions.[2] Nevertheless, many drawbacks still characterize this design concept (i.e., flame stability and ignition performances), in particular, if compared to older RQL combustors.

Payri, R., Novella, R., Carreres, M., Belmar-Gil, M, "Modeling gaseous non-reactive flow in a lean direct injection gas turbine combustor through an advanced mesh control strategy", Proceedings of the Institution of Mechanical Engineers, Part G: Journal of Aerospace Engineering 234(11):1788-1810, 2020 (author version).

doi: 10.1177/0954410020919619

Thus, further investigation in this injection-combustion strategy is required.

In the LDI concept described in this manuscript, the air is swirled upstream of a venturi section, and the fuel is injected radially into the airstream from the venturi throat section in order to produce a lean mixture.[3,4] Hence, the swirling air-flow is used both for atomizing the injected liquid jets, mixing the atomized sprays and generating a recirculating region downstream, which acts as an aerodynamic flame holder. Thus, good atomization and quick and uniform fuel-air mixing are achieved in a short period enabling low-temperature combustions with low NOx levels. Air blast atomizers, pressure atomizers, and hybrid atomizers are used depending on the flow pattern requirements.[2] Even though its main interest resides on liquid-fueled systems, swirling devices are extensively used in premixed and non-premixed gaseous systems as well.[5,6]

In the recent past, a significant effort has been made on modeling and simulating the swirling flow in gas turbine combustors regarding different injection strategies and swirler types.[7-14] Even though these flows are employed in most engine designs, its chaotic nature hinders both experimental measurements and numerical computations, implying several phenomena are still not understood.

On the one hand, experimental observation of spray breakup, mixing and combustion in swirling flows still present some challenges concerning the dense regime. Although some imaging methods have been developed over the last few years,[15-17] there still exist uncertainties in getting an accurate prediction for both carrier and disperse phases close to the nozzle exit. For this reason, most of the experimental techniques have been reduced to measurements in the diluted regime employing contrasted techniques such as LDV, PDA or LIF. The turbulent flow field within the combustor has been visualized for a long time using the Laser-Doppler Velocimetry (LDV) technique.[18,19] Nevertheless, the Phase Doppler Anemometry (PDA) technique irruption has allowed improving the comprehension of spray dynamics and droplet characteristics as it is used to characterize both gaseous and liquid phases statistics as mean and fluctuating velocity and diameter.[20-25]

On the other hand, a vast number of computational researches of swirling spray combustors have been carried out. Given the high turbulence and unsteadiness associated with the swirling motion inside the combustor, the Unsteady Reynolds-Averaged Navier Stokes (U-RANS) turbulence modeling approach precludes a complete analysis of the flow characteristics.[26-28] U-RANS simulations model the turbulence and only resolve statistically steady flow structures, failing in predicting turbulence fluctuation statistics accurately and, thus, resulting insufficient in to represent the complexity of lean combustors. Recently, some direct numerical simulation (DNS) investigations of swirling spray combustion have been performed[4, 29] in which all the scale structures of scalar and velocities fluctuations are solved. Nevertheless, these

Payri, R., Novella, R., Carreres, M., Belmar-Gil, M, "Modeling gaseous non-reactive flow in a lean direct injection gas turbine combustor through an advanced mesh control strategy", Proceedings of the Institution of Mechanical Engineers, Part G: Journal of Aerospace Engineering 234(11):1788-1810, 2020 (author version).

doi: 10.1177/0954410020919619

simulations are still limited to low Reynolds numbers since its expensive computational cost limits its application in practical flows. Therefore, Large Eddy Simulations (LES) has emerged as a realistic alternative and has been applied in most numerical studies in order to investigate the generation and evolution of fully transient coherent structures in swirl-stabilized combustors.[3,13,30-37] In LES, the governing equations are filtered to separate the large-scale turbulence, solved by the discretized equation; and small-scale turbulence, modeled through the sub-grid scales models to represent the effects of unresolved small-scale fluid motions.

The present work reports non-reactive U-RANS and LES simulations of a gaseous-fueled radial-swirled lean-direct injection (LDI) combustor utilizing CONVERGE™ CFD code by solving the complete inlet flow path through the swirl vanes and the combustor. In the last years, CONVERGE™ has been extensively used in the investigation of Internal Combustion engines[38-41] due to both its automated mesh generation and the adaptive mesh refinement algorithm, which allow to easily optimize the cell count to maximize accuracy and computational efficiency. Despite the wide application of AMR to flows involving shocks or chemical reactions, there have been fewer investigations regarding the implementation of AMR to turbulent flows. Nevertheless, some recent researches have been carried out to expand the use of this code to the Gas Turbine field.[42-43] The emphasis of this work is placed on the demonstration of the CONVERGE™ applicability to the multi-scale Gas Turbine engines field and the determination of an optimal mesh strategy through several grid control tools (i.e., local refinement, adaptive mesh refinement) allowing the exploitation of its benefits against traditional fixed mesh approaches in this kind of multi-scale problem. In this way, the main objective of this paper is to define a methodology to establish a meshing strategy that allows characterizing the gaseous flow field concerning gaseous fuel injections in a lean direct injection burner through several grid control tools. Such a strategy would provide the user with a more automated mesh generation to study this kind of problem with less computational resources than traditional approaches, without compromising accuracy. For this purpose, the Normalized Mean Square Error (NMSE) has been adopted to quantify the accuracy of turbulent numerical statistics regarding the agreement with the experimental database. The geometry here considered is the gaseous injection configuration of the CORIA burner, for which detailed measurements are available.[44]

In this way, the present investigation aims at facing two partial objectives. On the one hand, modeling the key features of swirling flow through an automatic mesh algorithm in CONVERGE™. In this regard, an investigation on how the adaptive mesh refinement technique allows employing moderate computing resources in predicting the complex swirling flow features is performed. On the other hand, assessing the behavior when coupling a given LES sub-grid scale model (i.e., Smagorinsky, Dynamic Smagorinsky, and Dynamic Structure) with the adaptive mesh refinement algorithm. To

Payri, R., Novella, R., Carreres, M., Belmar-Gil, M, “Modeling gaseous non-reactive flow in a lean direct injection gas turbine combustor through an advanced mesh control strategy”, Proceedings of the Institution of Mechanical Engineers, Part G: Journal of Aerospace Engineering 234(11):1788-1810, 2020 (author version).

doi: 10.1177/0954410020919619

explore this, each SGS model performance (CPU hours required to simulate the same amount of physical time) and predictive capability in capturing the vortex dynamics has been quantified considering both a coarse and a refined grid. On this point, the Dynamic Smagorinsky model has demonstrated the potential to provide more accurate computed time-averaged statistics when employing a sufficiently refined grid, while the Dynamic Structure model arises as the best option when dealing with a coarser mesh.

The paper is organized as follows. **Section 2** describes the model combustor, spatial discretization of the computational domain, and imposed boundary conditions. In **Section 3**, the influence of available grid control tools is evaluated to finally establish an optimal mesh strategy. Furthermore, the performance and accuracy of LES sub-grid scale models are here reported together with a LES quality assessment. **Section 4** discusses the simulation results and the predicted flow topology features within the combustion chamber. Finally, the conclusions are summarized in **Section 5**.

2. TEST CASE DESCRIPTION AND NUMERICAL SETUP

2.1. Description of the test case

The computational investigation has been carried out based on the experimental gaseous configuration of the CORIA burner,[44] whose 3D model is depicted in **Figure 1(a)**. This burner configuration contains four major components: a plenum to tranquilize the flow before entering the swirler, a radial-swirl injection system, a square cross-section combustion chamber (100x100x260mm) and, finally, a convergent exhaust to prevent air recirculation. The combustor employs a radial swirler, illustrated in **Figure 1(b)**, composed of 18 channels inclined at 45º with an external diameter of D = 20 mm. The swirler creates a swirling air flow in the combustion chamber, in which gaseous methane is injected through a tube (d = 4 mm) acting as fuel injector located in the center of the swirler. The injector may be operated with premixed or non-premixed methane (CH_4) and air inflows. In the premixed mode (see the left side of **Figure 2**), both plenum and fuel injector are fed with a full mixture of methane and air. On the other hand, in the non-premixed mode (see right side of **Figure 2**), pure methane is injected through the nozzle while the air enters the combustion chamber across the plenum.

Payri, R., Novella, R., Carreres, M., Belmar-Gil, M, "Modeling gaseous non-reactive flow in a lean direct injection gas turbine combustor through an advanced mesh control strategy", Proceedings of the Institution of Mechanical Engineers, Part G: Journal of Aerospace Engineering 234(11):1788-1810, 2020 (author version).

doi: 10.1177/0954410020919619

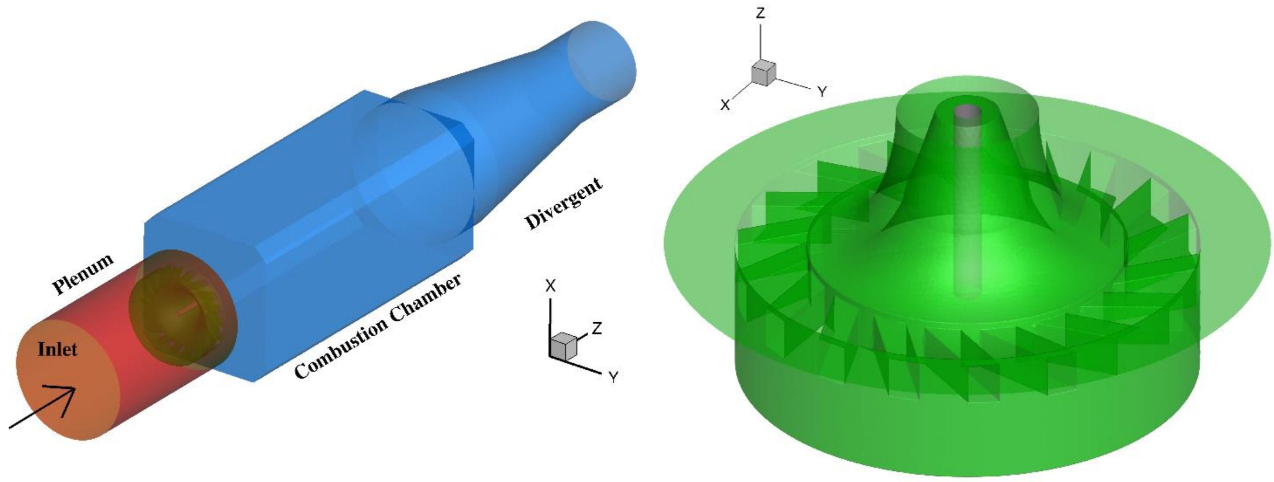

Figure 1. Overview of the CORIA single burner computational domain: the air plenum, the swirl-injection system, the combustion chamber, and the convergent exhaust (a). Zoom to the swirled injection system (b).

In this work, a premixed gaseous injection strategy has been simulated at ambient conditions (T = 298 K; p = 1atm). The operating condition corresponds to a global equivalence ratio of 0.75, where the swirler and the central jet are fed with 5.612 g/s (composed of 73.79% N_2, 22.04% O_2 and 4.168% CH_4) and 0.236 g/s (same composition) respectively of a fully mixed air-methane mixture.[44] Meanwhile, the inlet flow velocity of 28.8 m/s gives rise to a Reynolds number of 35,000 based on the mean diameter of the convergent inlet.

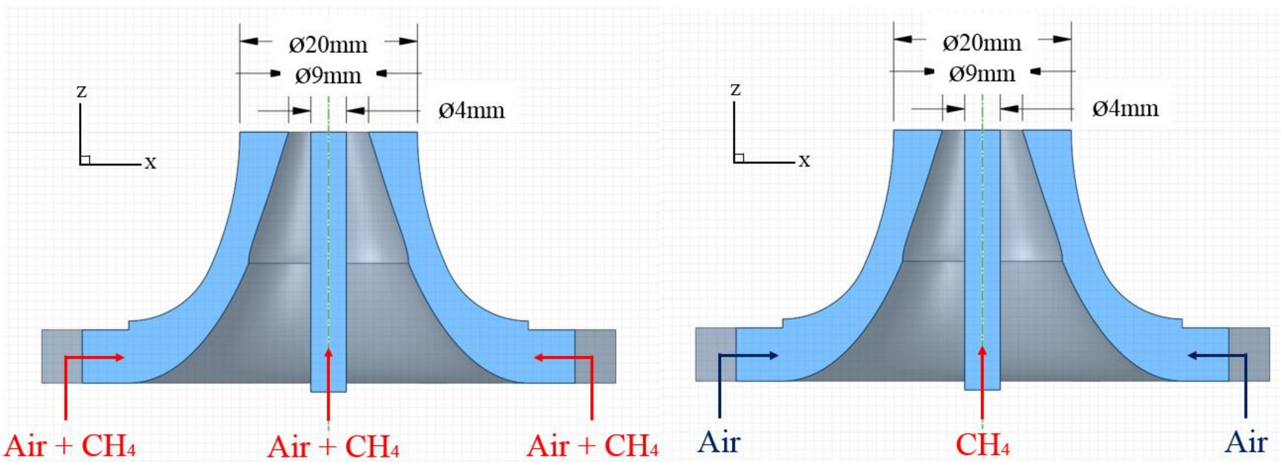

Figure 2. Sketch of the swirl-injection system showing both premixed (left) and non-premixed (right) injection strategies.

In the non-premixed mode[45], the operating condition corresponds to a global equivalence ratio of 0.75, where the swirler is fed with 5.43 g/s of air (77% N_2 and 23% O_2) whereas a pure methane (100% CH_4) mass flow rate of 0.234 g/s is imposed through the central jet, simulating the corresponding non-premixed experimental conditions[46].

As stated previously, CONVERGE™ CFD software[47] is employed to investigate the modeling strategies describing turbulence dynamics, in which the dynamics of the swirling flow within the combustor, governed by the Navier-Stokes Equations, are solved through the finite volume method. The computational domain includes the four components of the

Payri, R., Novella, R., Carreres, M., Belmar-Gil, M, "Modeling gaseous non-reactive flow in a lean direct injection gas turbine combustor through an advanced mesh control strategy", Proceedings of the Institution of Mechanical Engineers, Part G: Journal of Aerospace Engineering 234(11):1788-1810, 2020 (author version).

doi: 10.1177/0954410020919619

experimental test rig, as reported in **Figure 1(a)**. The axial direction is referred to as the *z*-axis, corresponding to the main flow direction, while the *x*-axis and *y*-axis denote the transverse directions.

2.2. Numerical Setup

This section presents a brief overview of the numerical algorithms, discretization schemes, and mesh manipulation considered in the current work. The simulations reported in this paper are performed with the commercial code CONVERGE™ in order to optimize the computational resources in this kind of multi-scale problem. CONVERGE™ code uses an innovative modified cut-cell Cartesian method that eliminates the need for the computational grid to be morphed with the geometry of interest, while still precisely representing the exact boundary shape.[48] This approach allows for the use of simple orthogonal grids and completely automates the mesh generation process.

In the present solver, all computed values are collocated at the center of the computational cell, where the conservation equations are solved using the finite volume method. A second-order-accurate spatial discretization scheme is used for the governing conservation equations, while a second-order implicit formulation is set for time discretization. The Rhie-Chow algorithm[49] is employed to prevent spurious oscillations (e.g., checker-boarding). Meanwhile, the transport equations are solved using the PISO algorithm. A variable time-stepping algorithm is used in the current study, where the time-step is automatically calculated each computational cycle, ensuring that the maximum CFL-number does not exceed 0.8 anywhere in the computational domain at any instant.

An automatic domain decomposition technique is employed, allowing for efficient load balancing throughout the calculation. CONVERGE™ includes several tools for controlling the grid size before and during a simulation:

- Base Size: side length of the hexahedral cells, from which the other grid control tools are defined.
- Fixed Embedding (FE): refines the grid at user-specified locations (areas) and times where a finer resolution is critical to the accuracy of the solution (i.e., the flow behavior within the small passages of the swirler), whereas allows the rest of the grid to remain coarse to minimize simulation time. An embedding scale (a positive integer) must be specified for each fixed embedding area defined, including the refinements of the cells adjacent to walls.
- Adaptive Mesh Refinement (AMR): automatically changes the grid based on fluctuating and moving conditions. Specifically, the AMR method adds embedding where the flow field is more under-resolved or where the sub-grid field is the largest without unnecessarily slowing the simulation with a globally refined grid. To do so, the AMR algorithm estimates the magnitude of the sub-grid field (ϕ'), computed as the difference between the actual field (ϕ) and the resolved field ($\bar{\phi}$), to determine where to add embedding. The scale of the sub-grid can be approximated by Eq. (1):

$$\phi' = -\frac{dx_k^2}{24}\frac{\partial^2\bar{\phi}}{\partial x_k \partial x_k} \tag{1}$$

Then, a cell is embedded if the absolute value of the sub-grid given by Eq. (1) is above a user-specified value (called threshold value in the remainder of this article). Conversely, a cell is released (i.e., the embedding is removed) if the absolute value of the sub-grid is below 1/5 of the user-specified value.[47]

All these grid control techniques refine (or coarsen) the base mesh by cutting the cell dimensions in half (or doubling them) for each level of refinement (i.e., a 2 mm of base mesh size with three levels of fixed embedding would be converted in 512 cells of 0.25 mm). In this work, the influence of the grid control tools has been evaluated through a parametric study presented in **Section 3.2**. For illustrating purposes, **Figure 3** shows the strategy followed in the mesh refinement through the selected grid-tools described previously.

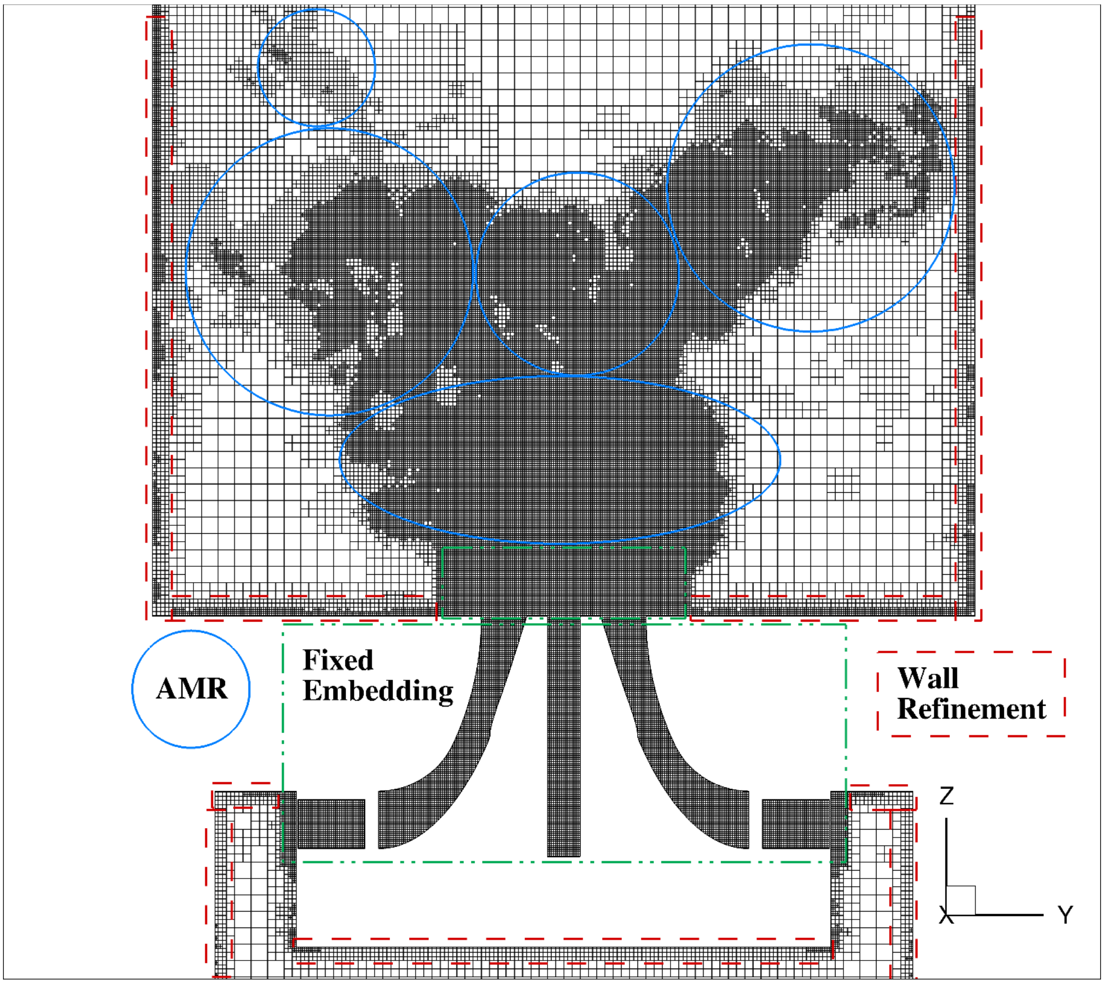

Figure 3. Slice in the computational domain for a LES simulation in CONVERGE™ illustrating the strategy considered in the mesh refinement: 3 levels of fixed embedding, 3 levels of AMR, and 2 layers with 2 levels of wall refinement.

Finally, U-RANS (i.e., the Standard, Realizable and RNG k-ε, and the LRR Reynolds Stress Model) and LES (i.e., the

Payri, R., Novella, R., Carreres, M., Belmar-Gil, M, "Modeling gaseous non-reactive flow in a lean direct injection gas turbine combustor through an advanced mesh control strategy", Proceedings of the Institution of Mechanical Engineers, Part G: Journal of Aerospace Engineering 234(11):1788-1810, 2020 (author version).

doi: 10.1177/0954410020919619

Smagorinsky, Dynamic Smagorinsky, and Dynamic Structure) modelling options for the treatment of turbulence have been applied separately to characterize the unsteady non-reacting flow field. Additionally, standard law of the wall profile is used to determine the tangential components of the stress tensor at the wall in U-RANS simulations, whereas the Werner and Wengle wall model is considered in LES. In this respect, AMR of y^+ was used to maintain the proper level of mesh near the wall ensuring y^+ values between 30 and 100 so that the wall models can work in a satisfactory way. The use of wall models in this kind of device dominated by the large-scale motions can be justified through several LES considering the same experimental test rig reported in the literature[50] in which a better agreement both in terms of pressure loss and velocity field when considering wall-models instead of resolving the boundary layers is described. Notwithstanding the Werner and Wengle wall model is suitable for dealing with cells located at both the viscous ($y^+ < 5$) and buffer ($5 < y^+ < 30$) sublayers, authors have preferred to avoid placing any cells in that conflictive region since approximation of wall models at the buffer sublayer can result in errors around 10-20% that might compromise the accuracy of the overall results. Meanwhile, the variable time step sizes resulting from the CFL restriction mentioned above are between $2\cdot10^{-6}$s - $4\cdot10^{-6}$s for U-RANS and $1\cdot10^{-6}$s – $2.5\cdot10^{-6}$s for LES, being the mean CFL number around 0.001. For typical simulations, mesh scaling of twice the baseline mesh size was used to stabilize the flow field until 50 ms before automatically scaling down to the base mesh size and starting the fixed embedding and AMR tools. The simulations were run for additional 100 ms to stabilize the overall mass flow rate and velocity fields (i.e., the parameters considered for checking the convergence in a statistical steady state) with the final mesh strategy. From here, temporal averages and higher-order moments started to be calculated. The statistics were computed during approximately 25 times the rotation flow scale (50 ms). This time scale is associated to some large coherent structures generated within the combustor and will be presented in **Section 4.1**. The overall CPU cost of the CONVERGE™ premixed-study was about 320k CPU hours on a computer cluster (Intel E5-2450 processors).

3. MESHING STRATEGY

3.1. Defining accuracy of a simulation: Normalized Mean Square Error (NMSE)

The results presented here contain the CONVERGE™ premixed cases for all turbulence approaches considered and meshes proposed. The turbulent field of a given variable obtained from U-RANS and LES simulations can be decomposed in the mean (time-averaged), and root mean square (fluctuation) values, evaluated respectively by Eq. (2) and Eq. (3):

Payri, R., Novella, R., Carreres, M., Belmar-Gil, M, “Modeling gaseous non-reactive flow in a lean direct injection gas turbine combustor through an advanced mesh control strategy”, Proceedings of the Institution of Mechanical Engineers, Part G: Journal of Aerospace Engineering 234(11):1788-1810, 2020 (author version).

doi: 10.1177/0954410020919619

$$\langle\psi(\vec{x})\rangle = \frac{1}{T_m}\sum_{n=1}^{N_T}\psi(\vec{x},t^n)\Delta t_m \tag{2}$$

$$\psi(\vec{x})_{RMS} = \sqrt{\langle\psi(\vec{x})^2\rangle - \langle\psi(\vec{x})\rangle^2} \tag{3}$$

where T_m is the recording duration (50 ms in most of the simulations), N_T is the number of time steps, and Δt_m is the value of the time step. It is important to remark that the RMS value calculated by Eq. (3) does not account for the sub-grid scale contribution, which is expected to slightly modify the real value but with no substantial influence in the results presented in this section.

The accuracy of a given simulation is measured through the evaluation of the Normalized Mean Square Error (hereafter referred to as *NMSE*), defined by Eq. (4) and widely used in literature to quantify CFD performance considering discrepancies between predicted and measured values:[51,52]

$$NMSE = \frac{(\phi_N - \phi_E)^2}{|\phi_N \phi_E|} \tag{4}$$

where ϕ_N is the numerical mean (time-averaged) or RMS value of a given flow variable calculated through CFD in a given spatial location, whereas ϕ_E denotes the same flow variable value obtained experimentally in the same location. A perfect model would have $NMSE = 0$. Even though the quality acceptance criteria for this metric strongly depends on what the data underlying represents, reference studies[53] state $NMSE < 4$ as an acceptable quality criterion for a predictive model. However, these are not definite guidelines, and it is essential to consider all performance measures in deciding on model acceptance. In this study, the computed *NMSE* value has proven its suitability for comparing the performance between different simulations.

The numerical mean (time-averaged) and RMS velocity components (i.e., axial, radial and tangential) have been computed at locations where experimental data are available[44]: in the centreline and at radial stations located at a given axial distance from the entrance of the combustion chamber, as shown in **Figure 4**.

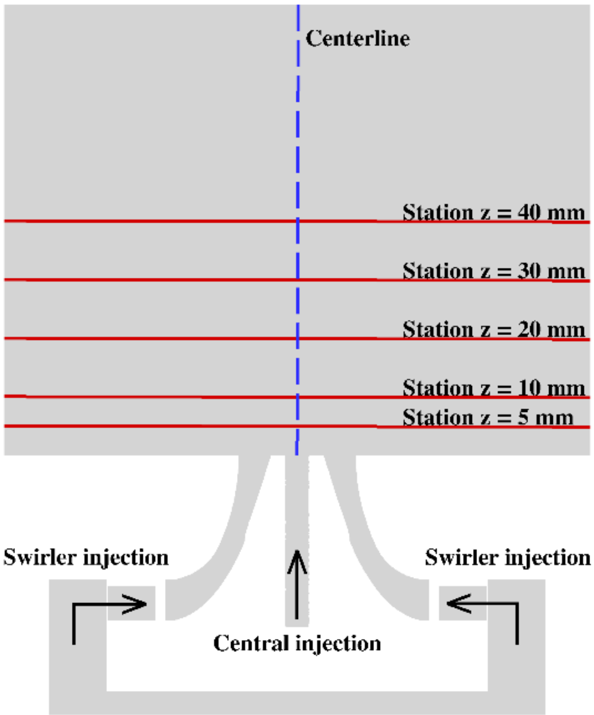

Figure 4. Overview of the measurement transverse cross-section where experimental data are available for comparison with CFD simulations: the centreline, and the radial stations located at five different axial positions.

The strategy followed to evaluate the prediction quality of a given CFD simulation is to obtain three differentiated NMSE values: one for the time-averaged axial velocity along the centerline (i.e., NMSE-Centerline), another for the mean of the time-averaged components velocity in all the stations (i.e., NMSE-Mean-Stations) and a last one for the same but considering the RMS values (i.e., NMSE-RMS-Stations). These three global values are obtained by averaging the discrete values obtained at each discrete location where experimental data is available. Please note that U-RANS k-ε simulations are expected to obtain higher values of *NMSE-RMS-Stations* since the governing equations are ensemble-averaged before being solved and the isotropic turbulence hypothesis is assumed, meaning few fluctuations are expected.

3.2. Methodology for meshing strategy

As already stated, one of the two main objectives of the investigation is to understand how different mesh layouts and turbulence resolution can impact on the prediction of the flow field within the burner. The accuracy of the results in terms of the *NMSE-Centerline-Value* (the most representative curve in this kind of burners) is reported and discussed for several mesh strategies through the evaluation of the available grid control tools. Given the high number of possible combinations between the potential meshing strategies and turbulence models, the simulations have been selected carefully to explore the tendency when modifying the parameters studied:

- On the one hand, the influence of the grid control tools is analyzed (see **Section 3.2.1**). For this study:
    - The Standard k-ε U-RANS turbulence model is employed since fewer cell count and faster simulations

Payri, R., Novella, R., Carreres, M., Belmar-Gil, M, "Modeling gaseous non-reactive flow in a lean direct injection gas turbine combustor through an advanced mesh control strategy", Proceedings of the Institution of Mechanical Engineers, Part G: Journal of Aerospace Engineering 234(11):1788-1810, 2020 (author version).

doi: 10.1177/0954410020919619

are expected (this choice will be justified in **Section 3.2.2**):

  - The base mesh size for the combustor was varied in all three dimensions, considering 2, 3, 4, 5, and 6 mm for each simulation.
  - The Fixed Embedding influence has been analyzed, by applying one layer and refinement level over every surface in the geometry and considering 0 and 3 levels in the complete region of the swirler and combustion chamber inlet.
  - AMR sensitivity was studied employing 0, 3, and 4 levels for velocity gradients for a fixed threshold set on 0.1.

  - The dynamic Smagorinsky LES turbulence model is considered for evaluating the influence of the AMR algorithm in a LES framework both in terms of the computational costs (CPU hours for simulating 200 ms) and the agreement with experimental data.

- On the other hand, U-RANS (i.e., Standard, Realizable and RNG *k*-*ε*, SST *k*-*ω* and LRR Reynolds Stress Model) and LES (i.e., Smagorinsky, Dynamic Smagorinsky, and Dynamic Structure) modelling options for the treatment of turbulence have been applied (see **Section 3.2.2**). The optimal mesh case setup extracted from the study mentioned above is employed to evaluate the influence of the U-RANS and LES turbulence models. Furthermore, for LES the base mesh size has been also reduced to 2 mm (i.e., smallest cells of 0.25 mm) and the wall refinement has been increased to two layers and levels.

3.2.1. Assessment of the CONVERGE grid control tools

A set of 11 standard *k*-*ε* U-RANS simulations performed through CONVERGE to analyse the base size influence together with the fixed embedding and AMR is summarized in **Figure 5**, for which the *NMSE-Centerline* value is represented. The lines join simulations that keep all the parameters constant (i.e., a given zone of influence and levels of fixed embedding, and a given threshold and levels of AMR) except for the base size. It is important to remark that the number of cells reported in CONVERGE is a result of time-averaging the instantaneous cell count during the same temporal window used to compute the turbulent statistics. As a consequence of the AMR action, the maximum and the minimum number of cells of a given simulation usually oscillates between ±5-8% about the mean value reported.

Payri, R., Novella, R., Carreres, M., Belmar-Gil, M, "Modeling gaseous non-reactive flow in a lean direct injection gas turbine combustor through an advanced mesh control strategy", Proceedings of the Institution of Mechanical Engineers, Part G: Journal of Aerospace Engineering 234(11):1788-1810, 2020 (author version).

doi: 10.1177/0954410020919619

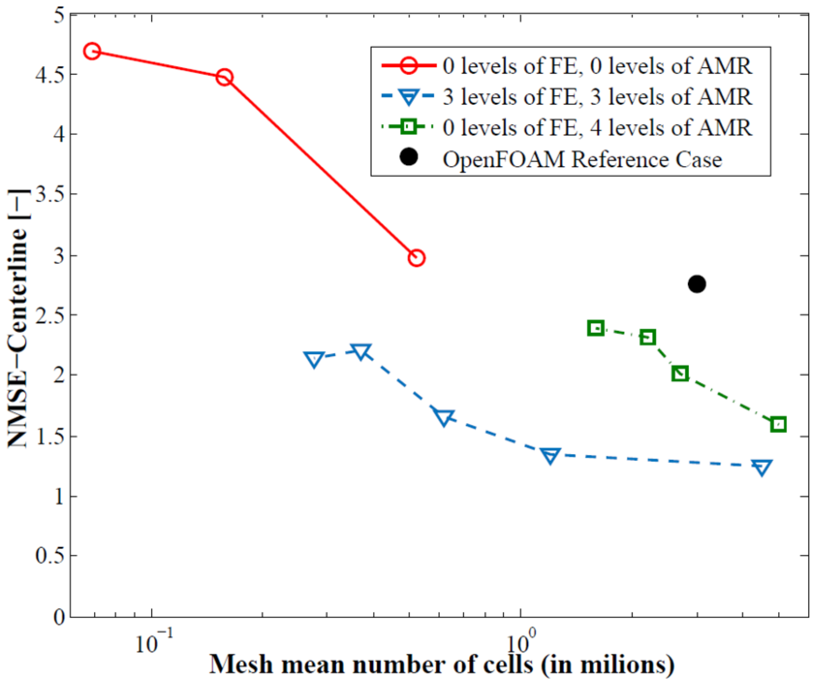

Figure 5. Influence of the grid control tools on the *NMSE-Centerline* value. Each line represents the variation of the base size for a given strategy of AMR and fixed embedding refinement.

From the examination of the grid tools impact in **Figure 5**, it may be stated that:

- When no fixed embedding or AMR is considered, the tendency to reduce the base size from 4 mm (i.e., 70,000 cells) to 2 mm (i.e., 525,000 cells) is towards a better agreement with experimental data, as expected. Nevertheless, the absence of any specific refinement causes a low resolution locally in the critical flow sections (i.e., the swirler and combustion chamber inlet), and unacceptable results are obtained with *NMSE-Centerline* values greater than 4.
- Regarding the application of three levels of fixed embedding and AMR, the baseline size was varied from 6 mm (i.e., 275,000 cells) to 2 mm (i.e., 4,500,000 cells). A clear improvement in the *NMSE* value compared with the previous non-locally refined strategy is observed. As expected, the *Normalized Mean Square Error* at the centerline presents better results as the base size is decreased up to 3 mm (i.e., the smallest cell size of 0.375mm). Nevertheless, note that no apparent improvement is shown when reducing the base size to 2 mm, then discarding the need to reduce the cell size as much in zones far from the injection region for U-RANS simulations.
- Last, the influence of removing the fixed embedding and letting the AMR algorithm be the sole tool in charge of mesh refinement is evaluated. For this task, the base size has been changed from 6 mm to 3 mm. The *NMSE-Centerline* value reported decreases monotonously as the base size is decreased, as expected. However, the improvement obtained is not compensated with the growth in the overall cell count, requiring three times more cells to compute with the same agreement than with the standard mesh setup. This can be attributed to the fact

Payri, R., Novella, R., Carreres, M., Belmar-Gil, M, "Modeling gaseous non-reactive flow in a lean direct injection gas turbine combustor through an advanced mesh control strategy", Proceedings of the Institution of Mechanical Engineers, Part G: Journal of Aerospace Engineering 234(11):1788-1810, 2020 (author version).

doi: 10.1177/0954410020919619

that the use of fixed embedding in regions where the presence of critical flow is expected (i.e., the swirler and the entrance of the combustor) acts as a trigger of the AMR in situations where otherwise would not be activated due to a low flow resolution. From here, a significant conclusion can be drawn: a base size greater than 3 mm is not fine enough to correctly model the turbulence scales through U-RANS, even if the smallest cells located in the crucial flow regions are finer than those of the corresponding 3 mm case (i.e., 0.375mm). This fact, together with the one extracted from the discussion above, results in an optimal mesh strategy for U-RANS cases consisting in a base size of 3 mm with 3 levels of both the AMR and the fixed embedding (in the swirler and entrance of the combustor region). Therefore, the Standard k-ε U-RANS simulation performed considering this optimal grid strategy is taken as reference for the following discussion about the turbulence model influence.

On the other hand, the *NMSE-Centerline* obtained in an additional OpenFOAM Standard k-ε U-RANS simulation considering a fixed unstructured 1.8-million cell mesh is also reported in **Figure 5** for being representative of a numerical study through traditional static grids. In this way, a similar mesh in terms of fixed refined cell sizes in those local regions where a finer resolution is critical to the accuracy of the solution (swirler and conical shape near the injector zone) was adopted. The results of this OpenFOAM simulation were post-processed in an identic way, obtaining good agreement with experiments both quantitatively (through the *NMSE-Centerline* and *NMSE-Mean-Stations* values) and qualitatively by direct visual comparison with the velocity field at the considered radial stations. When comparing the results of the CONVERGE optimal mesh case defined above with the OpenFOAM reference case (see **Table 1**), it can be concluded that the joint action of the AMR algorithm and the fixed embedding allows both an increase in accuracy and a reduction in computational resources.

	Computational cost			Agreement with experiments	
CFD Code	Cells	CPU h	Memory	NMSE-Centerline	NMSE-Mean-Stations
CONVERGE (optimal case)	1.2 M	2300	23 GB	1.35	2.32
OpenFOAM (reference case)	1.8 M	3700	12 GB	2.10	2.78

Table 1. Accuracy and computational requirements concerning the CONVERGE optimal mesh case and OpenFOAM reference case simulations.

Thus, the use of an automatic grid refinement tool in the vicinity of the high gradient of velocity allows:

- A smaller cell size at the entrance of the combustor (i.e., 0.375 mm for the optimal mesh defined in CONVERGE, as opposed to the 0.6 mm of OpenFOAM mesh), leading to a better performance of U-RANS models in modeling the smallest high-turbulent scales and therefore enhancing the agreement with experimental work (i.e., a NMSE-

doi: 10.1177/0954410020919619

Centerline of 1.35, against the 2.10 value obtained in OpenFOAM). Please note that, for a licit comparison in terms of precision, achieving the same element sizes in the fixed OpenFOAM mesh than those generated automatically by CONVERGE would imply more than 10 million cells.

- Keeping the overall cell count relatively low (i.e., a mean of 1,200,000 cells, versus the 1,800,000 cells in OpenFOAM mesh), which together with the structured cartesian mesh means an optimization of both the solution speed. Nevertheless, additional computational resources are required for runtime load balancing and re-meshing in CONVERGE in terms of RAM memory, so the performance of the two solvers (and meshing strategy) needs to be based both on RAM memory requirements and on the overall amount of CPU hours required to simulate the same amount of physical time (i.e., 200ms, as reported in **Section 2.2**). In this way, the lower number of elements in CONVERGE results in a reduction from 3.7k to 2.3k CPU hours (i.e., a reduction of nearly 40% in the computational resources) for the considered Standard k-ε U-RANS simulation, as showed in **Table 1**. In any case, it must be noted that the simulation performed in through CONVERGE demanded higher memory requirements because of its automatic mesh generation and adaptive mesh refinement algorithms.

Thus, a proper application of the grid control tools available in CONVERGE together with its automatic mesh generation algorithm has been demonstrated to be an attractive option to face this type of multi-scale problem.

On the other hand, the influence of the AMR algorithm has also been evaluated in a LES framework both in terms of the computational costs (CPU hours for simulating 200 ms) and the agreement with experimental data. In this respect, two different CONVERGE cases involving dynamic Smagorinsky Large Eddy Simulation (see Table 2) have been considered to directly evaluate the implications of considering the use of AMR through the three computed NMSE values (i.e., NMSE-Centerline, NMSE-Mean-Stations, and NMSE-RMS-Stations). Both cases present the same base mesh size (i.e. 2 mm) and the same 3 levels of fixed embedding in the swirler region. In the first case, 3 levels of AMR have been used. In the second case, the lack of AMR is compensated with an additional fixed embedding refinement in the near-injection zone, considering conical zones of influence and the progressive use of 3, 2 and 1 levels of refinement as the flow moves away from the injector. Please note that both the size of the zone of influence and the levels of refinement of this extra fixed embedding have been carefully selected trying to obtain a similar mesh number of cells than those regarding the LES with AMR.

	Computational cost			Agreement with experiments		
CASE (CONVERGE)	Cells	CPU h	Memory	NMSE-Centerline	NMSE-Mean-Stations	NMSE-RMS-Stations

Payri, R., Novella, R., Carreres, M., Belmar-Gil, M, "Modeling gaseous non-reactive flow in a lean direct injection gas turbine combustor through an advanced mesh control strategy", Proceedings of the Institution of Mechanical Engineers, Part G: Journal of Aerospace Engineering 234(11):1788-1810, 2020 (author version).

doi: 10.1177/0954410020919619

LES without AMR	16.7 M	27700	255 GB	0.85	2.82	0.37
LES with AMR	17.1 M	30600	290 GB	0.41	2.06	0.12

Table 2. Accuracy and computational requirements concerning the two dynamic Smagorinsky LES in CONVERGE to evaluate the influence of the AMR algorithm.

A better agreement with experimental data is obtained in the LES case with AMR both in the mean and fluctuating terms of the three velocity components through the three computed NMSE values. This can be then directly attributed to the 3 automatic refinement levels of AMR in the near injection region (see Figure 3) as opposed to the eventual 1 and 2 levels of fixed embedding that are present in some local zones of this same region in the LES without AMR. Nevertheless, it must be noted that the cost of this accuracy improvement is a moderate increasement on the computational requirements both in CPU hours (10% higher) and in RAM memory (15% higher), as showed in Table 2. Therefore, the AMR algorithm has proved to be able to distribute the cells in a proper way for this lean direct injection multi-scale problem in a LES framework.

3.2.2. Turbulence Models Influence

Regarding the turbulence approach considered, both U-RANS (for the optimal mesh case setup) and LES turbulence models influence are shown in **Figure 6, Figure 7** and **Table 1**, respectively. In this case, the three values of *NMSE* defined in **Section 3.1** are depicted for a given turbulence model with a given mesh strategy (i.e., a given mean number of cells). The first aspect worth mentioning is the difference in the mean overall cell count due to the specific behavior of each model with the same 3 levels of AMR and 0.1 threshold value defined. The higher number of cells in RNG k-ε, k-ω SST and LRR RSM models was expected since RNG formulation involved a modified form of the ε-equation which attempts to account for the different scales of motion through changes to the production term,[54] and RSM models required higher-level turbulence closures considering the anisotropy of the Reynolds stresses. Meanwhile, the specific SST k-ω formulation in the inner parts of the boundary layer and the extra non-physical turbulence levels provided in regions with large normal strain also result in a moderate higher number of cells. Because of that, these formulations modify the resolved and sub-grid field computed by the AMR algorithm leading to distinct sensibility responses to a given threshold.

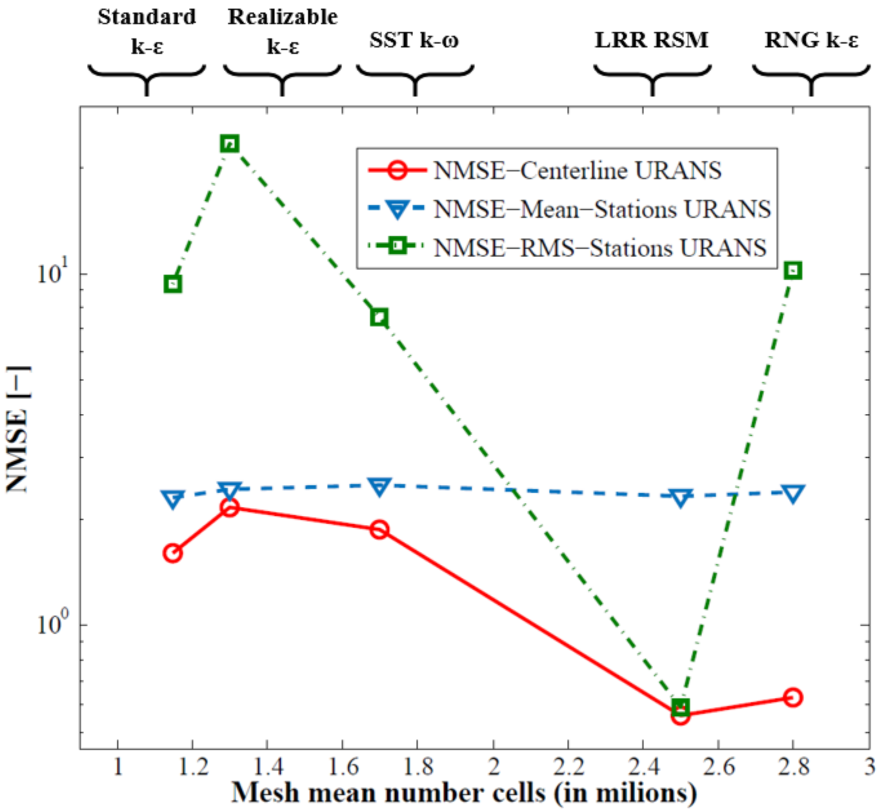

Figure 6. Influence of the U-RANS turbulence models on the *NMSE-Centerline*, *NMSE-Mean-Stations* and *NMSE-RMS-Stations* values.

In the case of the U-RANS turbulence models (see **Figure 6**), the Standard, RNG and Realizable *k-ε*, the SST *k-ω* and the Lauder-Reece-Rodi (LRR) Reynolds Stress Model (RSM) are tested. On the one hand, the Realizable, and Standard *k-ε* models, show a similar response in terms of keeping a relatively low number of cells (i.e., 1,200,000 cells). The Realizable variant was expected to present better results since it uses an improved formulation for the turbulent viscosity, thereby giving enhanced predictions for the spreading rate of jets, and superior ability to capture the mean flow of complex structures involving recirculation. Nevertheless, the Standard *k-ε* offered a better precision in the *NMSE-Centerline* value. Meanwhile, the application of the advanced SST *k-ω* model offered practically the same agreement with experiments that the Standard *k-ε* but presenting a 50% higher number of cells. This identical performance reported in the accuracy levels (i.e., *NMSE-Centerline* and *NMSE-Mean-Stations)* was expected since phenomena such as adverse pressure gradients and separating flows (where better behaviour according to the claims in the literature is expected) do not play a crucial role in the problem here studied and thus making worthless the improved near-wall performance of the *k-ω* model. On the other hand, the RNG *k-ε* and LRR RSM results are similar concerning both the total number of cells (i.e., 2,800,000 and 2,500,000 cells, respectively) and the great ability to predict the centreline velocity field. The RNG *k-ε* and LRR RSM models lead to slightly lower values of *NMSE-Centerline* (*NMSE-Centerline* < 1) than those obtained with Standard *k-ε*,

Payri, R., Novella, R., Carreres, M., Belmar-Gil, M, "Modeling gaseous non-reactive flow in a lean direct injection gas turbine combustor through an advanced mesh control strategy", Proceedings of the Institution of Mechanical Engineers, Part G: Journal of Aerospace Engineering 234(11):1788-1810, 2020 (author version).

doi: 10.1177/0954410020919619

but with more than twice the number of cells. Moreover, the *NMSE-Mean-Stations* reported for these models is slightly higher, so the preference in choosing the Standard *k-ε* (with acceptable *NMSE-Centerline* values) past the RNG is demonstrated. Additionally, the *NMSE-RMS-Stations* value (i.e., a parameter defined as a measurement of the ability of a given simulation to predict the velocity fluctuations) reported for the LRR RSM (*NMSE-RMS-Stations* = 0.60) is much better than the one obtained by *k-ε* models (*NMSE-RMS-Stations* > 10), as expected. Note that, as previously discussed, the two-equation turbulence models (*k-ε* and *k-ω*) are not capable to capture the fluctuations of the flow field accurately. Therefore, if predicting the fluctuating components (instantaneous field) of a given transient simulation plays a major role in the reliability of the results (e.g., characterization of the turbulent dispersion of liquid spray), the LRR-RSM will be the most appropriate way to approach the turbulence when computational resources are limited, and LES treatment is unaffordable.

Meanwhile, in LES framework, the turbulence resolution length scale or filter width $\Delta(\mathbf{x})$ is specified subjectively in a flow-dependent manner. For that reason, characterizing the dependence of predictions on Δ (directly related to the grid resolution dx_k, and hence to the ability of AMR algorithm to refine regions) must be part of the overall LES methodology. The final objective here should be to obtain that the fraction of the turbulent kinetic energy in the resolved motions is everywhere below a specified tolerance. To do so, the LES sub-grid scale models have been tested through six different simulations (see **Figure 7** and **Table 3**). The performance, the computational requirements and the predictive capability accuracy of Smagorinsky, Dynamic Smagorinsky, and Dynamic Structure SGS LES cases have been evaluated considering both the optimal mesh strategy (i.e., base size of 3 mm and smallest cells of 0.375 mm, hereinafter called coarse grid) and a more refined grid where the base mesh size has been reduced to 2 mm (i.e., smallest cells of 0.25 mm) and the wall refinement has been increased to two layers and levels. In general terms, an improvement in the *NMSE-Centerline* reported by the three refined-grid LES is detected, enhancing the prediction of the velocity field performed by U-RANS models. Furthermore, the *NMSE-RMS-Stations* value obtained indicates that the unsteadiness of the flow is captured more reliably (i.e., *NMSE-RMS-Stations* < 0.2).

Payri, R., Novella, R., Carreres, M., Belmar-Gil, M, "Modeling gaseous non-reactive flow in a lean direct injection gas turbine combustor through an advanced mesh control strategy", Proceedings of the Institution of Mechanical Engineers, Part G: Journal of Aerospace Engineering 234(11):1788-1810, 2020 (author version).

doi: 10.1177/0954410020919619

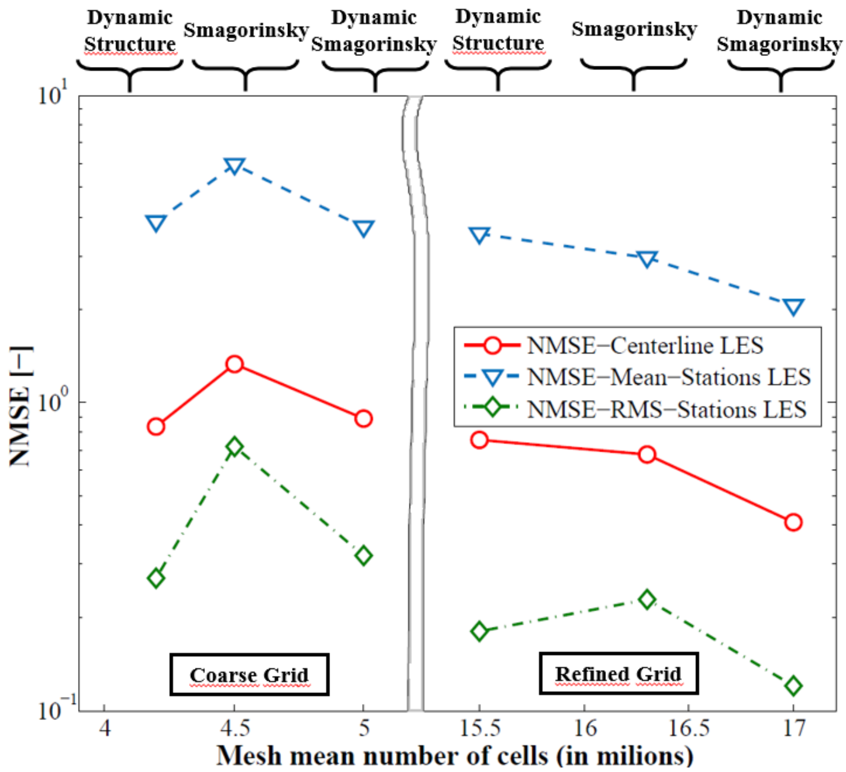

Figure 7. Influence of the SGS LES turbulence models on the *NMSE-Centerline*, *NMSE-Mean-Stations* and *NMSE-RMS-Stations* values.

On the one hand, the reduction in the base size carried out in the refined grid together with the higher sensitivity to a certain AMR threshold (for the same reason explained before) leads to total numbers of cells around 16,000,000. It is interesting to note how the ability when capturing smaller structures in LES acts as a trigger of the AMR. Furthermore, a difference in the response regarding the mean number of cells generated is observed: those SGS models that use the turbulent viscosity to model the sub-grid stress tensor (i.e., Smagorinsky and Dynamic Smagorinsky) tend to produce a slightly higher number of cells than those using an additional equation to compute the sub-grid kinetic energy (i.e., Dynamic Structure) for the same mesh strategy. Nevertheless, the evaluation of the convergence velocity shows that the Dynamic Structure one-equation model increases both the CPU cost and memory requirements for the presented simulation slightly since provides an independent SGS velocity scale and therefore account for non-equilibrium effects (see **Table 3**). It is interesting to note how this last consideration makes the one-equation Dynamic Structure model a more suitable option when dealing with coarser meshes, resulting in better values of *NMSE* than those obtained with zero-equation models.

	COARSE GRID (Base Size = 3 mm)			REFINED GRID (Base Size = 2 mm)		
SGS Model	Cells	CPU h	Memory	Cells	CPU h	Memory
Dynamic Structure	4.2 M	23400	200 GB	15.5 M	34200	300 GB

Payri, R., Novella, R., Carreres, M., Belmar-Gil, M, "Modeling gaseous non-reactive flow in a lean direct injection gas turbine combustor through an advanced mesh control strategy", Proceedings of the Institution of Mechanical Engineers, Part G: Journal of Aerospace Engineering 234(11):1788-1810, 2020 (author version).

doi: 10.1177/0954410020919619

Smagorinsky	4.5 M	18000	160 GB	16.3 M	27800	250 GB
Dynamic Smagorinsky	5.0 M	21600	180 GB	17.1 M	30600	290 GB

Table 3. Performance and computational requirements of the LES SGS models for the two meshing strategies considered.

On the other hand, in dynamic approaches, the coefficients of the SGS model are determined as part of the computation, based on the energy content of the smallest resolved scales. These dynamic models are usually driven by concepts of scale similarity: if the turbulent motion possesses scale similarity, then a model that considers this similarity should be suitable at different scales (i.e., for different values of filter widths Δ). In fact, Jiménez and Moser concluded that the physical basis for the good a posteriori performance of the Dynamic Smagorinsky sub-grid models in LES appears to be only weakly related to their ability to correctly represent the sub-grid physics.[55] The on-the-fly coefficient calculation of the dynamic models performed in this study (i.e., Dynamic Smagorinsky and Dynamic Structure) confirms the scale similarity of the flow within the burner since they report a more stable accuracy than the Smagorinsky model for different values of Δ when moving from coarse to refined grids (see **Figure 7**). Furthermore, it has been demonstrated that the fixed value of the Smagorinsky constant must be decreased in situations with high shear regions (shown in **Section 4.1**),[56] leading to more inaccurate predictions of the Smagorinsky model, especially when these regions are under-resolved (which seems to occur in the coarse mesh cases of this study).

From previous analysis and values reported in **Figure 7** and **Table 3** it can be concluded that: (1) the Dynamic Smagorinsky SGS model provides the best prediction ability on the computed time-averaged statistics when employing an sufficiently refined grid (when dealing with turbulence resolution length scale of 0.25 mm), and (2) the Dynamic structure model arises as the best option when dealing with a coarser mesh (turbulence resolution length scale of 0.375 mm). Therefore, the Dynamic Smagorinsky simulation considering the refined grid is taken for the LES quality assessment performed in **Section 3.3** and the transient analysis carried out in **Section 4.1** since it presents the best quality metrics for the three parameters computed.

3.3. LES quality assessment

The turbulence resolution in scale-resolved large eddy simulations (LES) depends on both the grid resolution and the modelling of the small scales. An important issue regarding LES is to know if the computational grid directly resolves a sufficient part of the turbulent flow energy. For such purpose, two criterions based on different approaches have been calculated for the Dynamic Smagorinsky LES (only the refined grid is considered for clarity) presented in **Section 3.2.2**:

- The criterion proposed by Pope[57] based on the turbulence resolution is currently one of the most accepted

Payri, R., Novella, R., Carreres, M., Belmar-Gil, M, "Modeling gaseous non-reactive flow in a lean direct injection gas turbine combustor through an advanced mesh control strategy", Proceedings of the Institution of Mechanical Engineers, Part G: Journal of Aerospace Engineering 234(11):1788-1810, 2020 (author version).

doi: 10.1177/0954410020919619

methods to quantify the quality of a LES in predicting the velocity field. This index of quality (IQ_k) expresses the contribution of the resolved part of the turbulent kinetic energy, that is, the ratio between resolved and total (modelled + resolved) turbulent kinetic energy. In this work, the resolved part is deduced from the filtered turbulent fluctuations, computed as $k_{res} = {}^1/_2 \left(\bar{u}^2_{x,RMS} + \bar{u}^2_{y,RMS} + \bar{u}^2_{z,RMS}\right)$, whereas the modelled part (sub-grid scale turbulent kinetic energy) is evaluated through Eq. (5):[58]

$$k_{mod} = \frac{1}{(C_m \Delta_e)^2} \nu^2_{sgs} \tag{5}$$

Where Δ_e is the filter width (i.e., the characteristic length of the grid cell: cube root of the cell volume), C_m is a model constant whose value has been taken as 0.091, and ν_{sgs} is the sub-grid scale viscosity. In this context, a good quality LES is defined when at least 80% of the turbulent kinetic energy is resolved ($IQ_k > 0.8$). **Figure 8(a)** shows the IQ_k criterion on the transversal x-cut exhibiting that the Pope requirement is globally satisfied inside the combustion chamber (particularly near the injection system where the turbulence is predominant) except near walls where the shears stress arises from modelled processes yielding unresolved boundary layers (not critical since the physical phenomena in these burners does not involve high adverse pressure gradients and separating flow in near-wall regions). The small sub-grid scale contribution to the computed RMS values stated in **Section 3.1** is here confirmed. Please note that a 0 value is also obtained when evaluating the IQ_k index within in areas where turbulence is not of critical interest such as the plenum and fuel line since no fluctuations are expected.

- A complementary index of quality based on the viscosity (IQ_ν) has been proposed[59] to describe LES resolution. This criterion evaluates the contribution relative to the laminar ν, the sub-grid ν_{sgs}, and the numerical ν_{num} viscosities according to Eq. (6):

$$IQ_\nu = \frac{1}{1 + \alpha_\nu \left(\frac{\nu_{sgs} + \nu + \nu_{num}}{\nu}\right)^n} \tag{6}$$

The two constants have been calibrated at $\alpha_\nu = 0.05$ and $n = 0.53$ through DNS results.[60] Celik et al.[59] suggested that IQ_ν value of 0.75 to 0.85 can be considered adequate for High-Reynolds-number flow. Results based on the computed IQ_ν value are shown in **Figure 8(b)** and reinforce the conclusion extracted from the Pope requirement, presenting acceptable index criteria values that demonstrate the consistency and the quality of the simulation.

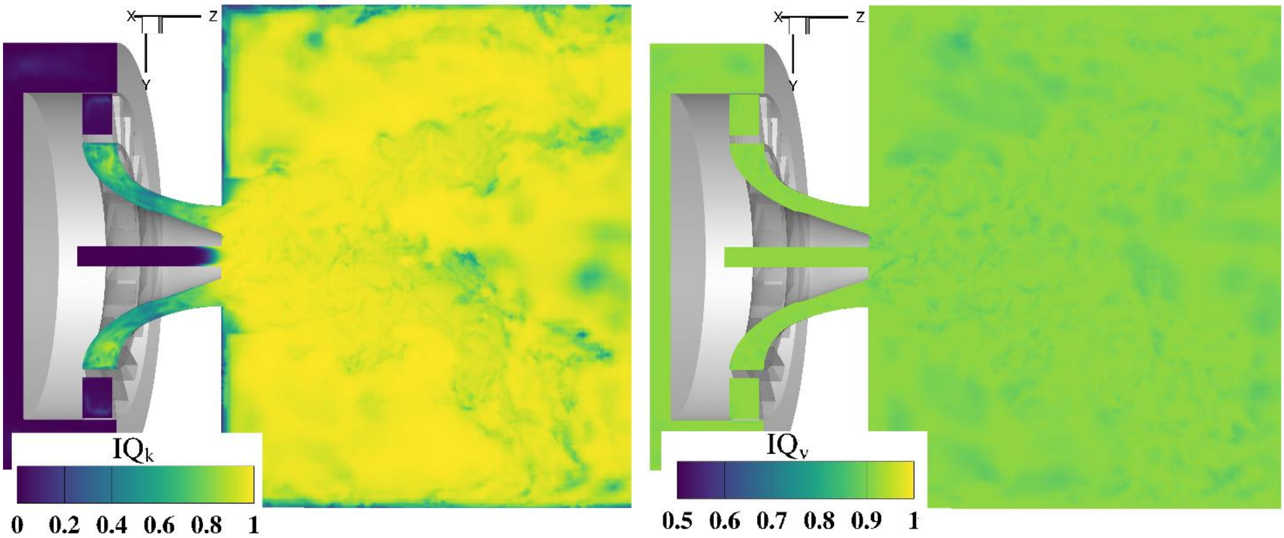

Figure 8. Assessment of the LES quality through two different criteria: Index based on the turbulent resolution IQ_k (a); Index based on the viscosity IQ_v (b).

Therefore, LES quality and reliability of non-reactive flow has been assessed based on measures of the turbulent resolution and viscosity. Such criteria confirm the validity of the AMR threshold defined for calculating the sub-grid field from the LES filtering and allows to certify the compatibility when combining LES with AMR implementation. Since controlling processes occur in the resolved large scales in this burner and considering both criteria are satisfied for the kind of grid, the low computational cost methodology here presented supports the adopted numerical setup for further liquid fuelled and reactive LES studies.

4. NUMERICAL RESULTS: VALIDATION AND DISCUSSION

4.1. Flow Visualization

An analysis of the time-evolving features in the combustor and a close examination of the flow near the vicinity of the injection system is carried out in the present section. From the discussion of **Section 3.3.2**, results presented in this section are focused on the Dynamic Smagorinsky LES case since it has exhibited the highest accuracy through the 3 *NMSE* values computed.

The degree of mixing depends mainly on the intensity of the swirl, defined by the swirl number S_W, which can be expressed according to Eq. (7):[61]

$$S_w = \frac{1}{R_{ext}} \frac{\int_0^{R_{ext}} \rho u_z u_\theta r^2 dr}{\int_0^{R_{ext}} \rho u_z^2 r dr} \tag{7}$$

When S_W exceeds a critical value in the swirler outlet region (typically 0.6 in such flows[62]), the phenomenon known as Vortex Breakdown Bubble (VBB) occurs, leading to the formation of a Central Toroidal Recirculation Zone. In the present work, the swirl number evaluated in the injection plane of the combustion chamber is 0.76, implying that the

Payri, R., Novella, R., Carreres, M., Belmar-Gil, M, "Modeling gaseous non-reactive flow in a lean direct injection gas turbine combustor through an advanced mesh control strategy", Proceedings of the Institution of Mechanical Engineers, Part G: Journal of Aerospace Engineering 234(11):1788-1810, 2020 (author version).

doi: 10.1177/0954410020919619

formation of a VBB is expected. **Figure 9(a)** shows the axial mean velocity field and streamlines pattern in a central *x*-cut plane allowing to illustrate the characteristic flow structures that are typically observed in a gas turbine combustor.[63] These include the Vortex Breakdown Bubble (VBB), which induces a Central Toroidal Recirculation Zone (CTRZ) with reverse flow, Corner Recirculation Zones (CRZ), and strong Shear Layers located at the interfaces between the Swirled Jet (SWJ) and both CTRZ and CRZ. All these unsteady, asymmetric and 3D flow features are influenced by the swirl strength and play an essential role in spray dispersion in axial and radial directions.

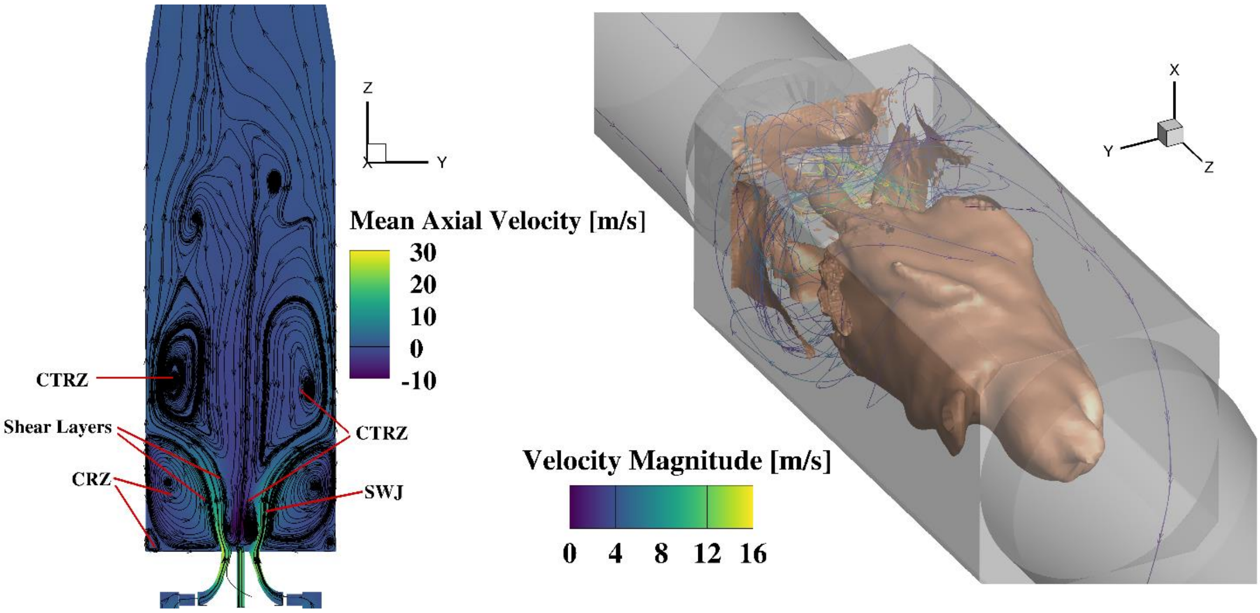

Figure 9. Mean (time-averaged) axial velocity field in a central *x*-cut plane and streamlines patterns showing the characteristic flow pattern within the CORIA LDI Combustor (a), and Vortex Breakdown Bubble identified using an iso-surface of zero mean streamwise velocity (b) at 200 ms.

LES simulations allow to identify the vortex structure and reveal the unsteady flow phenomena. The VBB can be described as the formation of a free stagnation point and a recirculation zone with a surrounding 3D spiral flow in the core. The axial location of the stagnation point (the first axial point with zero axial velocity) results from the equilibrium between the central jet and the reverse flow. **Figure 9(b)** shows the Vortex Breakdown Bubble identified through an iso-surface of zero mean streamwise velocity (iso-surface closed to the walls and upstream the combustion chamber has been blanked for the sake of clarity), and the streamlines, colored by the mean streamwise velocity, to demonstrate the spiral pattern of the flow. This swirling motion also creates an adverse pressure gradient in the axial direction that leads to the formation of the CTRZ. At high swirl numbers, a strong coupling is developed between axial and tangential velocity components and the axial adverse pressure gradient.[63] As the SWJ expands further downstream the combustion chamber, the momentum conservation implies decay of the tangential velocity, hence a decay of the radial pressure gradient, and thus a widening of the CTRZ forming its characteristic *bottle-neck* shape. In confined environments like the present

Payri, R., Novella, R., Carreres, M., Belmar-Gil, M, "Modeling gaseous non-reactive flow in a lean direct injection gas turbine combustor through an advanced mesh control strategy", Proceedings of the Institution of Mechanical Engineers, Part G: Journal of Aerospace Engineering 234(11):1788-1810, 2020 (author version).

doi: 10.1177/0954410020919619

combustor geometry, the SWJ also induces reverse flow regions on its outer part, known as Corner Recirculation Zones (CRZ).

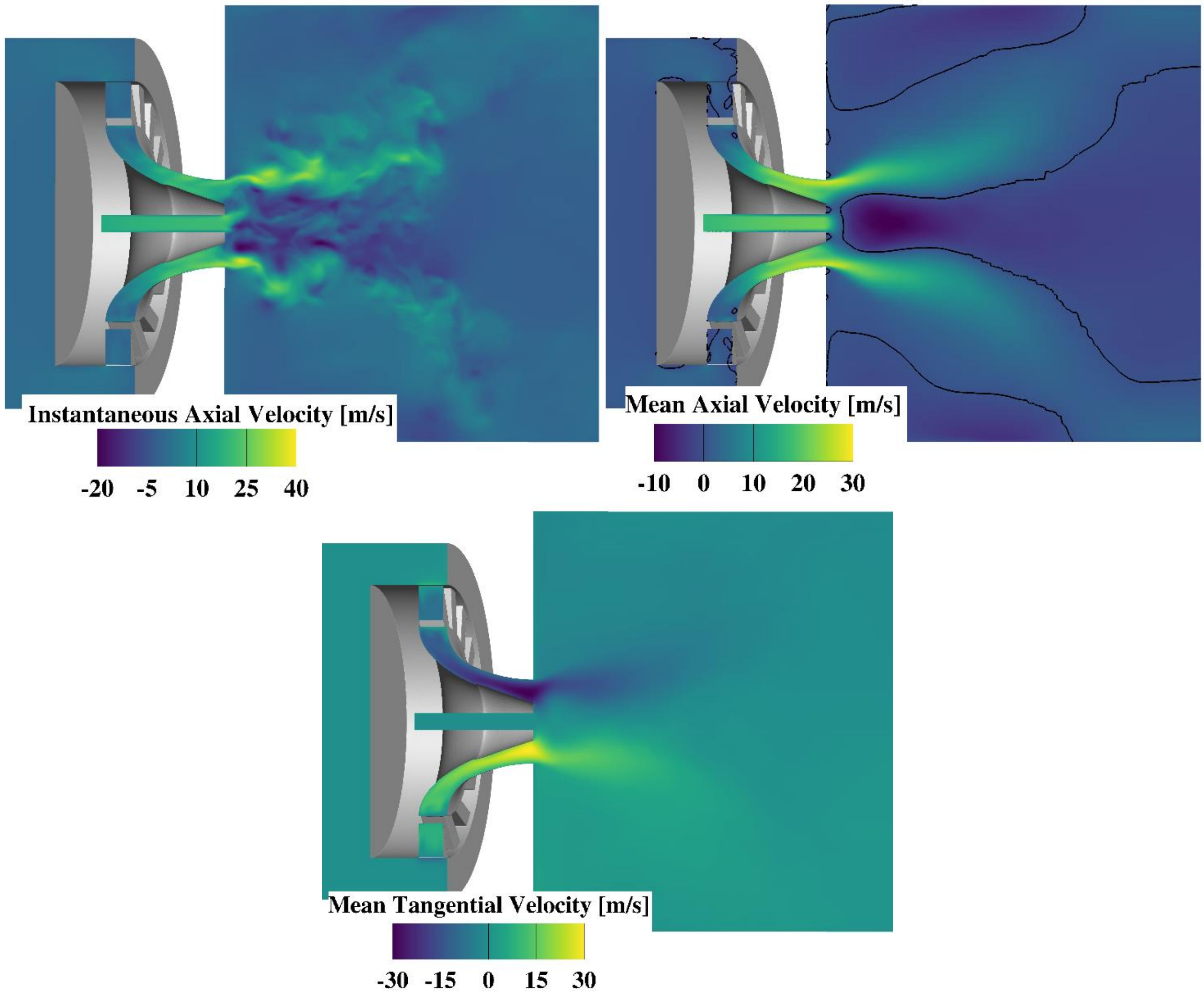

Figure 10. Contours of instantaneous (a) and time-averaged (b) axial velocity, and time-averaged tangential velocity (c) at 200 ms in the CORIA LDI Combustor.

Figure 10(a) shows the contour of the instantaneous axial velocity field at 200 ms, and **Figure 10(b)** depicts the time-averaged axial velocity field. Even though the recirculation zones shown in **Figure 10(b)** may appear to be confined regions with well-defined boundaries (zero-axial velocity regions are highlighted in black) the instantaneous flow field is much more dynamic and complex. Therefore, the time-averaged axial velocity field hides the highly general unsteadiness of the flow, turbulent mixing, and interactions that take place in this region. The boundary of the CTRZ is barely visible in the instantaneous field, which shows smaller and isolated recirculation zones with a high degree of unsteadiness. Furthermore, the contours show that the LES grid can resolve many small scale turbulent structures, as derived from **Section 3.3**. The high antisymmetric tangential velocity component observed in **Figure 10(c)** confirms the strong swirl

Payri, R., Novella, R., Carreres, M., Belmar-Gil, M, "Modeling gaseous non-reactive flow in a lean direct injection gas turbine combustor through an advanced mesh control strategy", Proceedings of the Institution of Mechanical Engineers, Part G: Journal of Aerospace Engineering 234(11):1788-1810, 2020 (author version).

doi: 10.1177/0954410020919619

number, calculated by Eq. (7), of the injection system at the injection plane reaching values as high as those obtained for the axial component, thus leading to the formation of the CTRZ. The generation of this CTRZ is crucial to provide enough residence time, and sufficiently high temperature and turbulent mixing to complete fuel combustion since it acts as an aerodynamic blockage and allows stabilizing the flame.

When the central vortex core starts precessing around the combustor axis of symmetry at a given frequency (f_{PVC}), it produces hydrodynamic instabilities. The frequency of precession is a function of the combustor design and the swirl intensity at the inlet. This unstable mode, typically related to the VBB, can be defined as the Precessing Vortex Core (PVC), and it is usually located along the outer boundary of the CTRZ. Further downstream of the injection position, turbulence breaks this large vortical structure into small scale ones, no coherent PVC being detected. The structure of the PVC generated within the combustor is well captured by LES and visualized in **Figure 11** through an iso-surface of the unsteady pressure field. The PVC presents an asymmetric shape around the central axis and tends to align with it near the inlet, but when it reaches the stagnation point, it forms a spiral pattern further downstream in the axial direction.

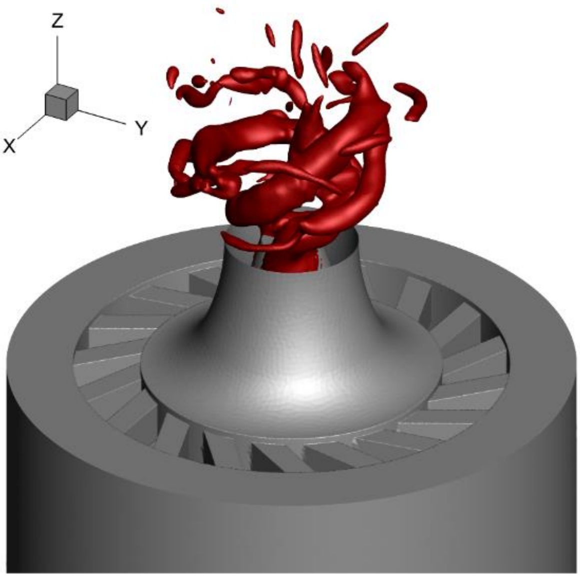

Figure 11. Instantaneous visualization of the Precessing Vortex Core identified through a pressure iso-surface of the instantaneous pressure $\bar{p} = 101.1$ kPa at 200 ms.

Meanwhile, a rotation time scale associated with the PVC can be defined to identify some unsteady flow structures, as shown in Eq. (8):

$$\tau_{rot} = \frac{2\pi R_i}{u_{\theta,i}} \tag{8}$$

where R_i is the mean radius of the convergent inlet and u_θ is the mean tangential velocity component in the inlet plane of the combustion chamber (see **Section 2.1** for geometric details). For the combustor here investigated, the rotation time

Payri, R., Novella, R., Carreres, M., Belmar-Gil, M, “Modeling gaseous non-reactive flow in a lean direct injection gas turbine combustor through an advanced mesh control strategy”, Proceedings of the Institution of Mechanical Engineers, Part G: Journal of Aerospace Engineering 234(11):1788-1810, 2020 (author version).

doi: 10.1177/0954410020919619

scale evaluated though Eq. (8) at the combustion chamber inlet is around 2 ms.

To end with the transient analysis, **Figure 12** shows a snapshot of the vorticity magnitude field in a central *x*-cut plane captured by LES. Vorticity is related to the flow circulation and presents a large magnitude, especially in the outer shear layer. Well-organized large vortical structures, arising from the shear layers downstream of the dump plane (z = 0 plane), are observed to be convected downstream, and then become disordered and dissipated into small-scale eddies due to the strong CTRZ. Hence, the high turbulence-intensity region developed at the combustion chamber inlet as a precursor of liquid atomization and enhanced mixing is confirmed again.

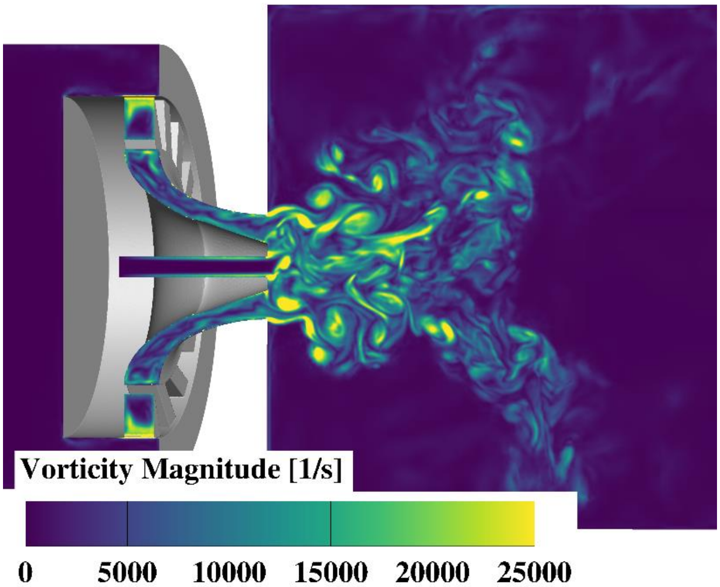

Figure 12. Snapshot of the vorticity magnitude field in a central *x*-cut plane at 200 ms in the Dynamic Smagorinsky LES.

4.2. Mean features

The statistically averaged flow field (obtained by Eq. (2) and Eq. (3)) allows comparing numerical and experimental time-averaged velocity profiles. **Figures 13**, **14** and **15** show the radial distributions (x = 0 corresponds to the centerline of the chamber) of the mean velocity components, and its root-mean-square (representing the turbulent velocity or fluctuations), at five axial locations (z = 5, 10, 20, 30 and 40 mm) within the CORIA burner. The results here presented correspond to the best numerical setups obtained from the methodology shown in **Section 3**: the 3M elements LRR Reynolds Stress Model U-RANS and 17M elements Dynamic Smagorinsky LES in CONVERGE are plotted together with both experimental data[44] and a 24M elements Dynamic Smagorinsky LES through AVBP found in the literature.[50] AVBP is a massively parallel finite-volume code for compressible reacting flows on unstructured fixed grids.[64] AVBP results are here taken as a reference to illustrate the predictive capabilities of the actual CFD codes employed by the scientific community to resolve the problem considered, especially taking into account that the experimental uncertainty of the

Payri, R., Novella, R., Carreres, M., Belmar-Gil, M, "Modeling gaseous non-reactive flow in a lean direct injection gas turbine combustor through an advanced mesh control strategy", Proceedings of the Institution of Mechanical Engineers, Part G: Journal of Aerospace Engineering 234(11):1788-1810, 2020 (author version).

doi: 10.1177/0954410020919619

velocity measurements has not been reported.

In a first look, the global flow topology and the amplitude of the mean and RMS velocity profiles are well reproduced. The mean velocity profiles (left side of **Figures 13**, **14** and **15**) obtained in CONVERGE™ show that the computed velocity field is, qualitatively, in good agreement with experiments and AVBP simulations throughout the five stations. Both the U-RANS and the LES seem to accurately capture the jet opening angle, denoted by the peaks of the mean velocity components around x = 10 mm. Meanwhile, the turbulent velocity, given by the root mean square value (i.e., the RMS depicted on the right side of the **Figures 13**, **14** and **15**), is slightly over-predicted in all the simulations for axial and radial components. This could partly be attributed to the fact that the PIV resolution used for measurements is 1mm,[44] which is larger than the LES filter size in the near-injection zone, resulting in smaller measured RMS values due to averaging effect within the probe. Results show stronger turbulent velocities close to the chamber inlet, but an abrupt decay as the flow moves downstream. The different fluctuations profiles among three components up to 20 mm indicate the presence of an anisotropic Reynolds stress distribution produced by the strong swirling flow.

Payri, R., Novella, R., Carreres, M., Belmar-Gil, M, "Modeling gaseous non-reactive flow in a lean direct injection gas turbine combustor through an advanced mesh control strategy", Proceedings of the Institution of Mechanical Engineers, Part G: Journal of Aerospace Engineering 234(11):1788-1810, 2020 (author version).

doi: 10.1177/0954410020919619

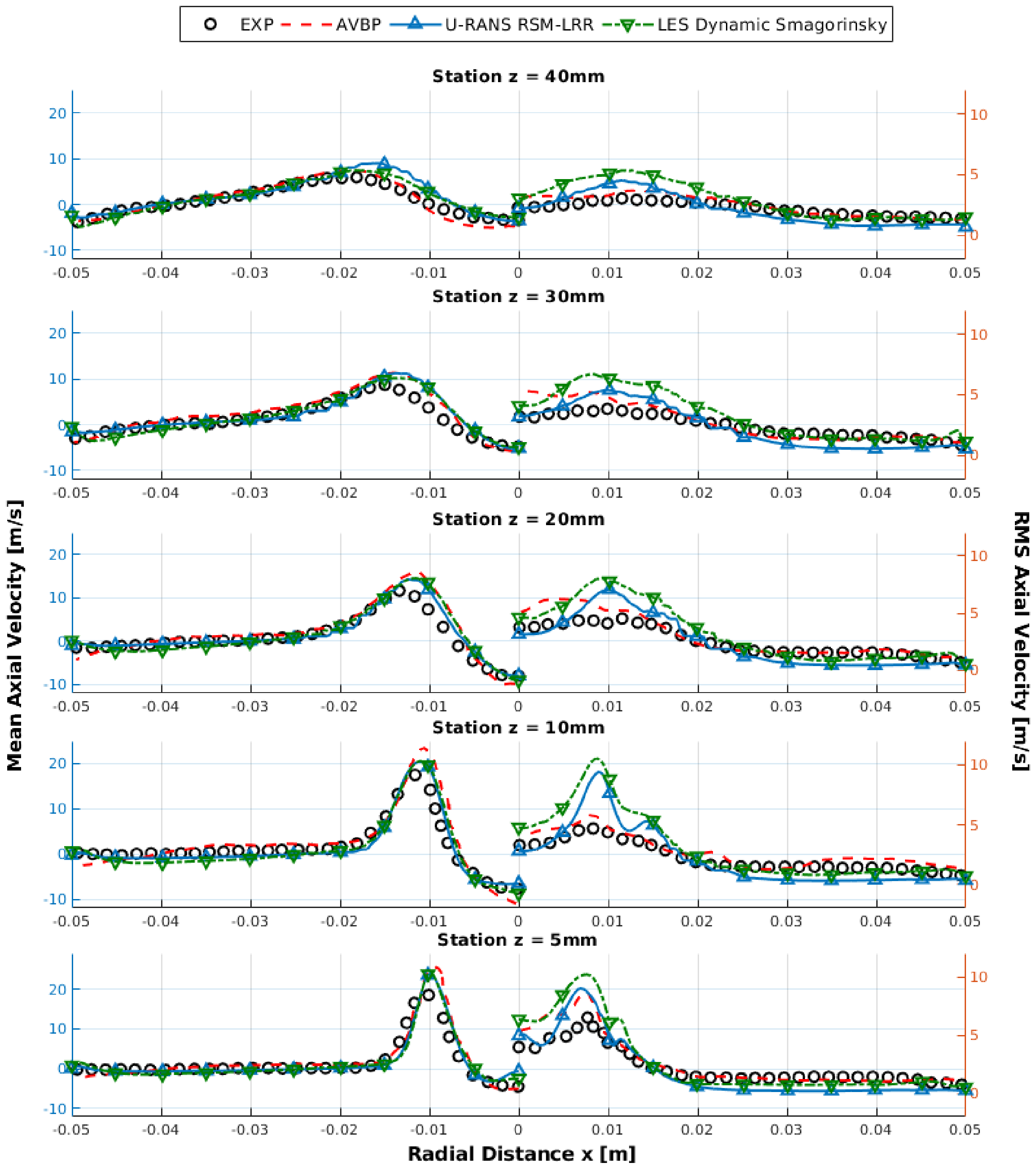

Figure 13. Mean and RMS Axial Velocity profiles obtained in U-RANS and LES simulations with CONVERGE™ at five axial locations.

The highest axial velocity is located in the SWJ, at the point where it reaches the combustion chamber. The jet opening is first limited due to the presence of the PVC resulting in a narrow CTRZ while further downstream (where the large structure has disappeared) the SWJ is fully opened. The mean axial velocity peak observed at the location *z* = 5 mm in **Figure 13** flattens out as the flow reaches stations far away from the combustion chamber inlet due to the expansion of the recirculation zone in the central region. Moreover, the computed axial velocity at the station *z* = 5 mm denotes a slightly stronger penetration of the central jet at *x* = 0, which appreciable modifies the velocity profile since a strong

doi: 10.1177/0954410020919619

gradient is found near the stagnation point. Results also show the negative axial velocities in the central and corner regions, confirming the existence of recirculation zones. It is also interesting to note that the time-averaged position of the CTRZ moves upstream towards the wall between the central jet and the SWJ.

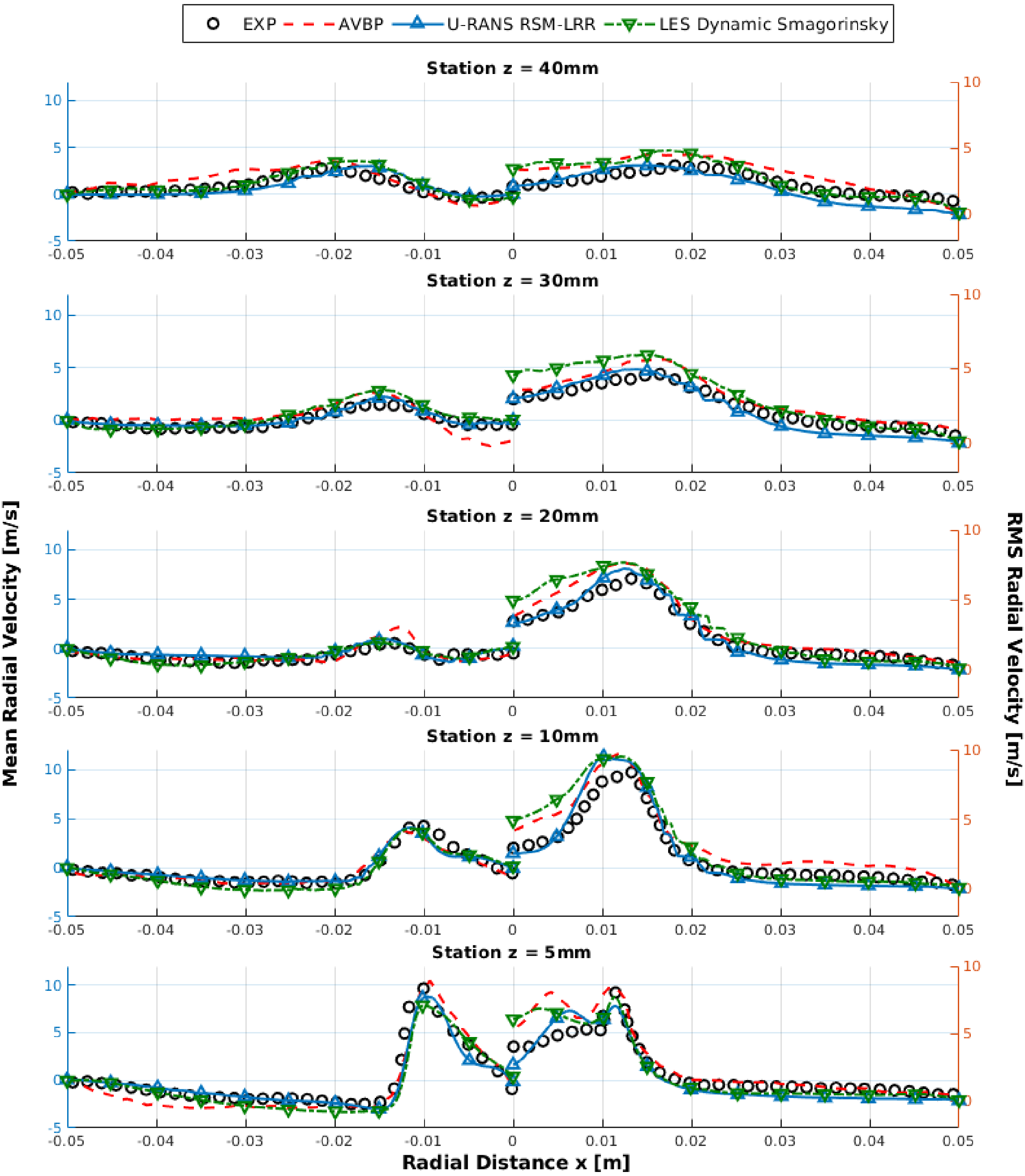

Figure 14. Mean and RMS Radial Velocity profiles obtained in U-RANS and LES simulations with CONVERGE™ at five axial locations.

The computed results of **Figure 14** exhibit the positive mean radial velocities in the main flow passage generated as a consequence of the incoming flow from the swirler spread outward from the central axis under the effect of the centrifugal force. Furthermore, the quick decrease of the high velocity of the central jet injection (visible on the axial velocity

Payri, R., Novella, R., Carreres, M., Belmar-Gil, M, "Modeling gaseous non-reactive flow in a lean direct injection gas turbine combustor through an advanced mesh control strategy", Proceedings of the Institution of Mechanical Engineers, Part G: Journal of Aerospace Engineering 234(11):1788-1810, 2020 (author version).

doi: 10.1177/0954410020919619

component of **Figure 13**), characterized by an abrupt decrease near the stagnation point implies a rapid increase of the radial component the conservation of the mass flow rate. Nevertheless, the mean radial velocity presents a lower magnitude than the axial and tangential components, and therefore, a quicker expansion downstream of the combustion chamber inlet.

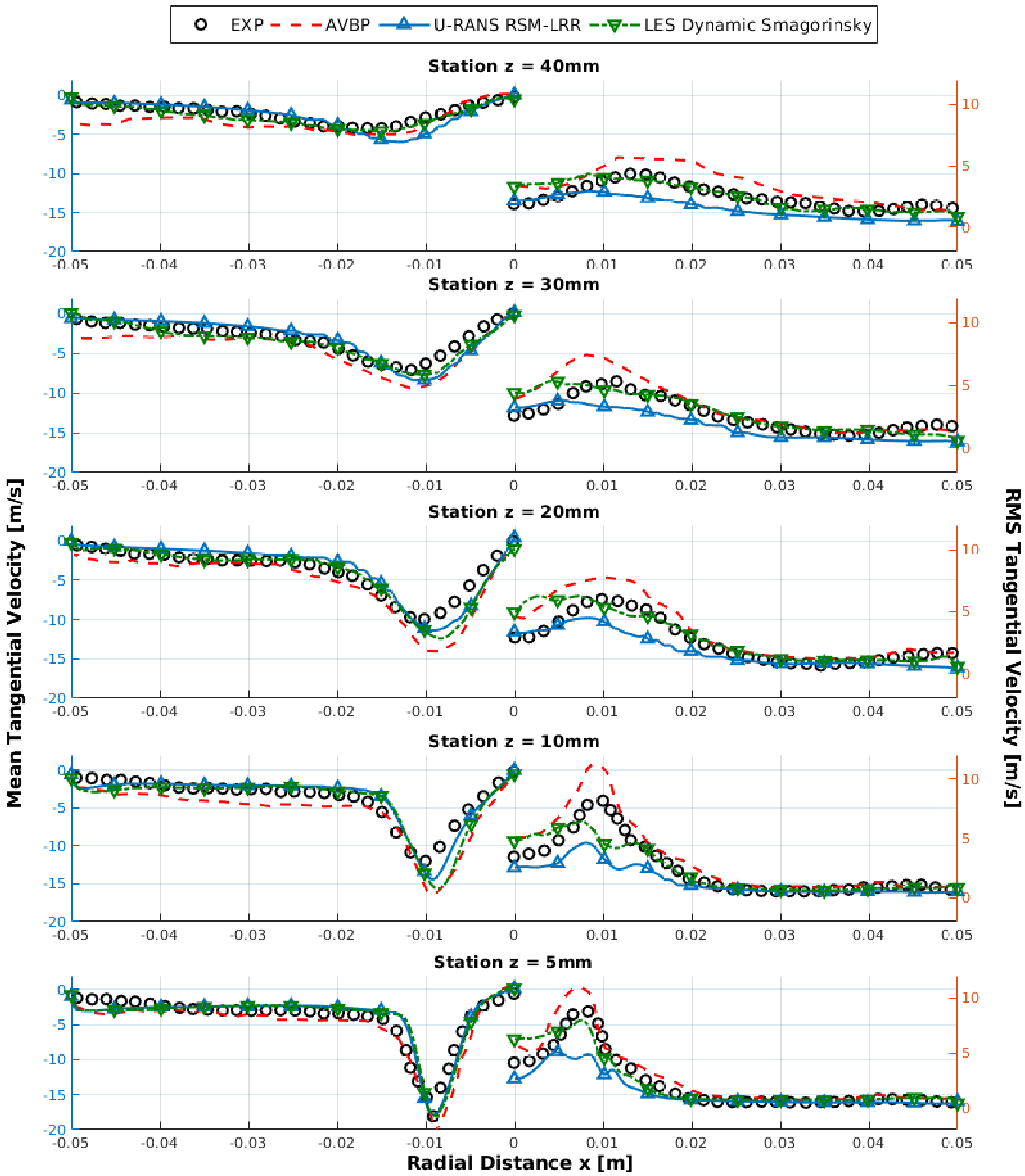

Figure 15. Mean and RMS Tangential Velocity profiles obtained in U-RANS and LES simulations with CONVERGE™ at five axial locations.

Regarding the mean azimuthal velocity profiles shown in **Figure 15**, the flow motion in the central region of the first axial stations is similar to a solid-body rotation and a free vortex structure, as observed in the PVC in **Section 4.1**.

Payri, R., Novella, R., Carreres, M., Belmar-Gil, M, "Modeling gaseous non-reactive flow in a lean direct injection gas turbine combustor through an advanced mesh control strategy", Proceedings of the Institution of Mechanical Engineers, Part G: Journal of Aerospace Engineering 234(11):1788-1810, 2020 (author version).

doi: 10.1177/0954410020919619

Meanwhile, further downstream, the peak of mean tangential velocity moves outward, and a solid vortex profile is established. Besides, it is observed that the magnitude of the mean tangential velocities (which primarily represents the swirl of the flow) is much higher than the corresponding to the mean radial velocities, even in stations further downstream from the combustion chamber inlet, as expected in these high swirling flows combustors. Furthermore, the distributions of the RMS velocity components illustrate the flapping motion of the central jet and SWJ indicating that a high turbulence-intensity region is developed at the combustion chamber inlet, where large velocity fluctuations are produced because of the PVC existence and the strong turbulent mixing in the shear layers between the incoming-recirculation flows.

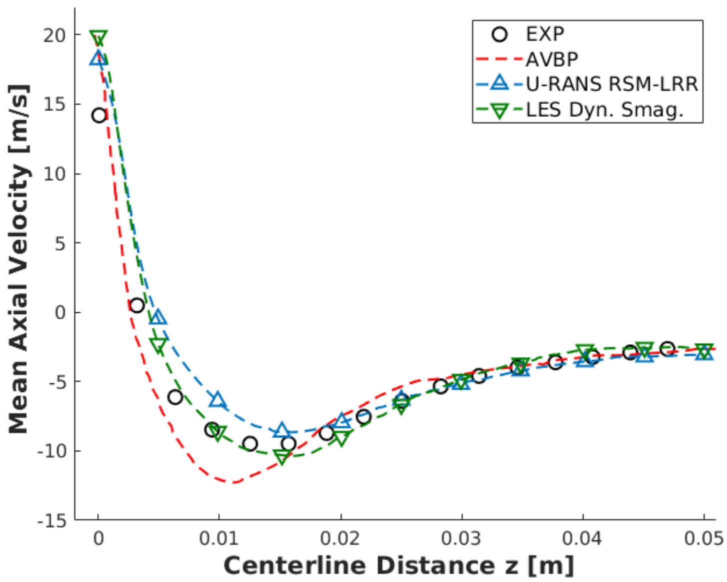

Figure 16. Mean Axial Velocity Profile along with the central axis of the burner. The *NMSE-Centerline* value reported is shown for each simulation.

Finally, the mean axial velocity profile along the central axis of the burner is shown in **Figure 16** for the same two simulations exposed previously. Please note that the experimental values here presented are those used to compute the *NMSE-Centerline* reported in **Section 3.1**. The greater ability of the Dynamic Smagorinsky LES to capture the axial velocity along the centerline shown in **Section 3.2.2** through the *NMSE-Centerline* can be appreciated here. The increase in the turbulent scales solved from U-RANS to LES can significantly improve the central jet penetration prediction, but the position of the stagnation point (i.e., the axial location with zero axial velocity) is still not fully recovered, exhibiting an offset of about 1 mm with experiments, as the one reported with the AVBP but in the opposite direction. Generally, the mean axial velocity is lightly over-predicted in the two cases along the first 10 mm but fully recovered downstream.

In the view of the results, the defined methodology allows simulating the swirling flow of a gaseous-fueled radial-swirled lean-direct injection (LDI) combustor with the same accuracy and predictive capabilities reported in the literature at a

Payri, R., Novella, R., Carreres, M., Belmar-Gil, M, “Modeling gaseous non-reactive flow in a lean direct injection gas turbine combustor through an advanced mesh control strategy”, Proceedings of the Institution of Mechanical Engineers, Part G: Journal of Aerospace Engineering 234(11):1788-1810, 2020 (author version).

doi: 10.1177/0954410020919619

lower computational cost. Additionally, after this study on the grid control tools, this methodology shapes a more automated modelling procedure than the standard employed by the scientific community. For these reasons, the presented methodology could be extrapolated to perform industrial simulations for design studies of realistic Gas Turbine engines.

5. CONCLUSIONS

An academic gas turbine combustor with premixed gaseous injection has been modeled through U-RANS and LES simulations employing the commercial CFD code CONVERGE, which provides advanced mesh handling features, including AMR algorithms. The main setup characteristics of the code have been described, focusing on the determination of an optimal mesh strategy through adaptive mesh refinement, and the exploitation of its benefits against traditional fixed mesh approaches in this kind of multi-scale problem. The applicability of CONVERGE, together with AMR algorithm, has been demonstrated to be an interesting option to face this type of multi-scale problem. A methodology has been presented to evaluate the influence on the accuracy of the grid control tools through a parametric study. The main findings of the present work are summarized as follows:

- The Normalized Mean Square Error has been adopted and systematically applied as a validation metric to quantify the existing discrepancies between the CFD numerical results and the available experimental data, proving to be a promising indicator to the quality of different meshing strategies.
- From a complete grid-tool parametric study carried out for U-RANS cases, a well-defined mesh strategy has been established to work out this multi-scale problem. The automatic cartesian meshing algorithm together with the joint action of both fixed embedding and Adaptive Mesh Refinement used in the present investigation, has allowed capturing the critical regions of high-velocity gradients enabling a larger base mesh size in areas where it was not required. This results in:
    - An optimization of the use of the computational resources, since a fewer number of cells are needed to obtain similar *NMSE* values to those of traditional fixed meshes utilized by the authors in OpenFOAM and reported in the literature through AVBP.
    - Better accuracy of the simulations carried out with the presented methodology in CONVERGE in terms of the *NMSE* for a given mean cell count due to an optimal mesh layout according to the flow characteristics.
- Meanwhile, in the LES framework:
    - The AMR algorithm has proved to be able to distribute the cells in a proper way for this lean direct

Payri, R., Novella, R., Carreres, M., Belmar-Gil, M, "Modeling gaseous non-reactive flow in a lean direct injection gas turbine combustor through an advanced mesh control strategy", Proceedings of the Institution of Mechanical Engineers, Part G: Journal of Aerospace Engineering 234(11):1788-1810, 2020 (author version).

doi: 10.1177/0954410020919619

    injection multi-scale problem A better agreement with experimental data is obtained in the LES case with AMR both in the mean and fluctuating terms of the three velocity components through the three computed NMSE values. Nevertheless, it must be noted that the cost of this accuracy improvement is a moderate increasement on the computational requirements both in CPU hours and in the RAM memory required.

    - LES quality and reliability of non-reactive flow has been assessed based on measures of the turbulent resolution and viscosity, reinforcing the selected turbulence resolution length scale. Such criteria confirm the validity of the AMR threshold defined for calculating the sub-grid field from the LES filtering and allows to certify the compatibility when combining LES with AMR implementation.
    - The Dynamic Smagorinsky sub-grid scale model has provided the best prediction ability on both the computed time-averaged statistics and the dynamic behaviour of the turbulent flow scales when employing a sufficiently refined grid, while the non-viscous Dynamic Structure model arises as to the best option when dealing with a coarser mesh.
    - The interaction of those SGS models that use the turbulent viscosity to model the sub-grid stress tensor (i.e., Smagorinsky and Dynamic Smagorinsky) with the AMR algorithm have demonstrated to produce a higher number of cells than those using an additional equation to compute the sub-grid kinetic energy (i.e., Dynamic Structure) for the same mesh strategy. The independent SGS velocity scale considered by the Dynamic Structure model modify the resolved field, and thus alleviates the sub-grid field computed by the AMR algorithm.

- Finally, the study demonstrates that CONVERGE numerical code can resolve the complex swirling flow features and the recirculation flow regions with reasonable accuracy. Agreement with experimental data was obtained both in U-RANS and LES in terms of predicted location and size of the CTRZ and CRZ as well as time-averaged and RMS values for velocity components. Nevertheless, LES outcomes confirm its potential to provide more accurate representations of the inherently unsteady large structures formed within the combustor, such as the vortex breakdown bubble (VBB) and the Precessing Vortex Core (PVC).

The outcome from the present research work is expected to be of interest for defining a suitable meshing strategy for modelers in the field of multi-scale gas turbine combustors. It should be noted that, although the meshing strategy here defined has been applied for solving non-reactive cases, this methodology can be considered as a suitable ground and can be extrapolated to more specific simulations involving multiphase and reactive flows.

Payri, R., Novella, R., Carreres, M., Belmar-Gil, M, “Modeling gaseous non-reactive flow in a lean direct injection gas turbine combustor through an advanced mesh control strategy”, Proceedings of the Institution of Mechanical Engineers, Part G: Journal of Aerospace Engineering 234(11):1788-1810, 2020 (author version).

doi: 10.1177/0954410020919619

ACKNOWLEDGEMENTS

This work was partly sponsored by the program “Ayuda a Primeros Proyectos de Investigación (PAID-06-18), Vicerrectorado de Investigación, Innovación y Transferencia de la Universitat Politècnica de València (UPV), Spain”. We thankfully acknowledge the computer resources at Altamira Supercomputer and the technical support provided by Universidad de Cantabria (RES FI-2018-1-0012 and FI-2018-2-0029) in the frame of the Spanish Supercomputing Network. On the other hand, the support given to Mr. Mario Belmar by Universitat Politècnica de València through the “FPI-Subprograma 2” grant within the “Programa de Apoyo para la Investigación y Desarrollo (PAID-01-18)” is gratefully acknowledged.

The authors would also like to thank Dorian Reale-Caron, Maël Barrué and Carlos Moreno for their support.

REFERENCES

1. Madden P. CAEP Combustion Technology Review Process and CAEP NOx Goals. In: FORUM-AE, 2 July 2014.
2. Lefebvre AH. Gas turbine combustion. 3rd ed. Taylor and Francis, 1998.
3. Patel N, Kırtas M, Sankaran V, et al. Simulation of spray combustion in a lean-direct injection combustor. *Proc Combust Inst* 2007; 31: 2327–2334.
4. Luo K, Pitsch H, Pai MG, et al. Direct numerical simulations and analysis of three-dimensional n-heptane spray flames in a model swirl combustor. *Proc Combust Inst* 2011; 33(2): 2143–2152.
5. Masri AR, Pope SB and Dally BB. Probability density function computations of a strongly swirling nonpremixed flame stabilized on a new burner. *Proc Combust Inst* 2000; 28(1): 123–131.
6. Johnson MR, Littlejohn D, Nazeer WA, et al. A comparison of the flowfields and emissions of high-swirl injectors and low-swirl injectors for lean premixed gas turbines. *Proc Combust Inst* 2005; 30(2): 2867–2874.
7. Sankaran V and Menon S. LES of spray combustion in swirling flows. *J Turbul* 2002; 3: 011.
8. Jones WP, Marquis AJ and Vogiatzaki K. Large-eddy simulation of spray combustion in a gas turbine combustor. *Combust Flame* 2014; 161(1): 222–239.
9. Ding G, He X, Xue C, et al. Preliminary design and experimental verification of a triple swirler combustor. *Proc IMechE Part G: J Aerospace Engineering* 2015; 229(12): 2258–2271.
10. Menon S and Patel N. Subgrid Modeling for Simulation of Spray Combustion in Large-Scale Combustors. *AIAA*

J 2006; 44(4): 709–723.

11. Wang P, Platova NA, Fröhlich J, et al. Large Eddy Simulation of the PRECCINSTA burner. *Int J of Heat Mass Transfer* 2014; 70: 486–495.

12. Cordier M, Vandel A, Cabot G, et al. Laser-induced spark ignition of premixed confined swirled flames. *Combust Sci Technol* 2013; 185(3): 379–407.

13. Patel N and Menon S. Simulation of spray-turbulence-flame interactions in a lean direct injection combustor. *Combust Flame* 2008; 153: 228–257.

14. Bang B, Kim Y, Jeong S, et al. Theoretical model for swirling thin film flows inside nozzles with converging-diverging shapes. *Appl Math Modell* 2019; 76: 607-616.

15. Linne M, Paciaroni ME, Hall T, et al. Ballistic imaging of the near field in a diesel spray. *Exp Fluids* 2006; 40(6): 836–846.

16. Desantes JM, Salvador FJ, Lopez JJ, et al. Study of mass and momentum transfer in diesel sprays based on X-ray mass distribution measurements and on a theoretical derivation. *Exp Fluids* 2011; 50(2): 233–246.

17. Reddemann MA, Mathieu F and Kneer R. Transmitted light microscopy for visualizing the turbulent primary breakup of a microscale liquid jet. *Exp Fluids* 2013; 54(11).

18. Chen RH and Driscoll JF. The role of the recirculation vortex in improving fuel-air mixing within swirling flames. *Symp (Int) Combust* 1989; 22(1): 531–540.

19. Presser C, Gupta AK and Semerjian HG. Aerodynamic characteristics of swirling spray flames: Pressure-jet atomizer. *Combust Flame* 1993; 92: 25–44.

20. Tacina KM, Chang C, He ZJ, et al. A Second Generation Swirl-Venturi Lean Direct Injection Combustion Concept. In: *50th AIAA/ASME/SAE/ASEE Conf*, Cleveland, USA, 28-30 July 2014.

21. Bulzan DL. Structure of a swirl-stabilized combusting spray. *J Propul Power* 1995; 6: 1093-1102.

22. Sommerfeld M and Qiu H. Experimental studies of spray evaporation in turbulent flow. *Int J Heat and Fluid Flow* 1998; 19: 10–22.

23. Hadef R and Lenze B. Measurements of droplets characteristics in a swirl-stabilized spray flame. *Exp Therm Fluid Sci* 2005; 30(2): 117–130.

24. Soltani MR, Ghorbanian K, Ashjaee M, et al. Spray characteristics of a liquid–liquid coaxial swirl atomizer at different mass flow rates. *Aerosp Sci Technol* 2005; 9(7): 592–604.

25. Tratnig A and Brenn G. Drop size spectra in sprays from pressure-swirl atomizers. *Int J Multiphase Flow* 2010;

Payri, R., Novella, R., Carreres, M., Belmar-Gil, M, "Modeling gaseous non-reactive flow in a lean direct injection gas turbine combustor through an advanced mesh control strategy", Proceedings of the Institution of Mechanical Engineers, Part G: Journal of Aerospace Engineering 234(11):1788-1810, 2020 (author version).

doi: 10.1177/0954410020919619

36(5): 349–363.

26. Asgari B and Amani E. A multi-objective CFD optimization of liquid fuel spray injection in dry-low-emission gas-turbine combustors. Appl Energy 2017; 203: 696–710.

27. Liu NS, Shih TH and Wey CT. Numerical Simulations of Two-Phase Reacting Flow in a Single-Element Lean Direct Injection (LDI) Combustor Using NCC. NASA/TM, 2011; 217031.

28. Wey T and Liu NS. Simulation of a Single-Element Lean-Direct Injection Combustor Using Arbitrary Polyhedral Mesh. In: *50th AIAA/ASME/SAE/ASEE Conf*, Cleveland, USA, 28-30 July 2014.

29. Moureau V, Domingo P and Vervisch L. From Large-Eddy Simulation to Direct Numerical Simulation of a lean premixed swirl flame: Filtered laminar flame-PDF modeling. *Combust Flame* 2011; 158(7): 1340–1357.

30. Caraeni D, Bergström C and Fuchs L. Modeling of liquid fuel injection, evaporation and mixing in a gas turbine burner using large eddy simulations. Flow Turbul Combust 2001; 65(2): 223–244.

31. Icardi M, Gavi E, Marchisio D, et al. Validation of LES predictions for turbulent flow in a Confined Impinging Jets Reactor. *App Math Modell* 2011; 35(4): 1591-1602.

32. Sanjosé M, Riber E, Gicquel L, et al. Large Eddy Simulation of a Two-Phase Reacting Flow in an Experimental Burner. Direct and Large-Eddy Simulation. *ERCOFTAC*, Springer, 2010, pp. 345-351.

33. Kırtaş M, Patel N, Sankaran V and Menon S. Large-Eddy Simulation of a Swirl-Stabilized, Lean Direct Injection Spray Combustor. In: *Proc Turbo Expo (ASME)*, Barcelona, Spain, 8-12 May 2006.

34. Sankaran V and Menon S. Vorticity-scalar alignments and small-scale structures in swirling spray combustion. *Proc Combust Inst* 2002; 29(1): 577–584.

35. Lebas R, Menard T, Beau PA, et al. Numerical simulation of primary break-up and atomization: DNS and modelling study. *Int J Multiphase Flow* 2009; 35(3): 247–260.

36. Zhou Y, Huang Y and Mu Z. Large eddy simulation of the influence of synthetic inlet turbulence on a practical aeroengine combustor with counter-rotating swirler. *Proc IMechE Part G: J Aerospace Engineering* 2019; 233(3): 978–990.

37. Hasti VR, Kundu P, Kumar G, et al. Numerical Simulation of Flow Distribution in a Realistic Gas Turbine Combustor. In: *AIAA/ASME/SAE/ASEE Conf*, Ohio, USA, 9-11 June 2018.

38 Torregrosa AJ, Broatch A, García-Tíscar J, et al. Modal decomposition of the unsteady flow field in compression-ignited combustion chambers. *Combust Flame* 2018; 188: 469-482.

39. Broatch A, Novella R, Gomez-Soriano J, et al. Numerical methodology for optimization of compression-ignited

Payri, R., Novella, R., Carreres, M., Belmar-Gil, M, “Modeling gaseous non-reactive flow in a lean direct injection gas turbine combustor through an advanced mesh control strategy”, Proceedings of the Institution of Mechanical Engineers, Part G: Journal of Aerospace Engineering 234(11):1788-1810, 2020 (author version).

doi: 10.1177/0954410020919619

engines considering combustion noise control. *SAE Paper* 2019; 11: 625-642.

40. Xu L, Bai XS, Jia M, et al. Experimental and Modeling Study of Liquid FuelInjection and Combustion in Diesel Engines with a Common Rail Injection System. *Appl Energy* 2018; 230: 287-304.

41. Broatch A, Olmeda P, Margot X, et al. Numerical simulations for evaluating the impact of advanced insulation coatings on H2 additivated gasoline lean combustion in a turbocharged spark-ignited engine. *Appl Therm Eng* 2019; 148: 674-683.

42. Kumar G and Drennan S. A CFD Investigation of Multiple Burner Ignition and Flame Propagation with Detailed Chemistry and Automatic Meshing. In: *52nd AIAA/SAE/ASEE Conf*, Salt Lake City, USA, 25– 27 July 2016.

43. Drennan S and Kumar G. Using LES Simulations to Predict Pilot Fuel Split Emissions Effects in an Industrial Gas Turbine Combustor with Automatic Meshing. In: *55th AIAA Aerosp Sci*, Grapevine, USA, 9th – 13th January 2017.

44. Cordier M, Vandel A, Cabot G, et al. Laser-induced spark ignition of premixed confined swirled flames. *Combust Sci Tech* 2013; 185(3): 379–407.

45. Payri, R., Novella, R., Carreres, M., and Belmar-Gil, M. Study about the influence of an automatic meshing algorithm on numerical simulations of a Gaseous-Fueled Lean Direct Injection (LDI) Gas Turbine Combustor in Non-Reactive conditions. In: *29th Conference on Liquid Atomization and Spray Systems*, Paris ,France, 2nd - 4th September 2019.

46. Esclapez, L., Riber, E., Cuenot, B. *Proc Combust Inst* 2005; 35(3): 3133–3141

47. CONVERGE 2.4 Manual. Convergent Science, Inc., Middleton, 2017.

48. Senecal PK, Richards KJ, Pomraning E, et al. A New Parallel Cut-Cell Cartesian CFD Code for Rapid Grid Generation Applied to In-Cylinder Diesel Engine Simulations. *SAE Paper* 2007; 776–790.

49. Rhie CM and Chow WL. Numerical study of the turbulent flow past an airfoil with trailing edge separation. *AAIA J* 1983; 21(11): 1525–1532.

50. Barré D, Kraushaar M, Staffelbach G, et al. Compressible and low Mach number LES of a swirl experimental burner. *3rd INCA Colloquim* 2013; 341: 277–287.

51. Gousseau P, Blocken B and van Heijst GJ. Quality assessment of Large-Eddy Simulation of wind flow around a high-rise building: Validation and solution verification. *Comput Fluids* 2013; 79: 120–133.

52. Hanna SR, Tehranian S, Carissimo B, et al. Comparisons of model simulations with observations of mean flow and turbulence within simple obstacle arrays. *Atmos Environ* 2002; 36: 5067–5079.

53. Hanna SR, Hansen OR, and Dharmavaram S. FLACS CFD air quality model performance evaluation with Kit

Payri, R., Novella, R., Carreres, M., Belmar-Gil, M, "Modeling gaseous non-reactive flow in a lean direct injection gas turbine combustor through an advanced mesh control strategy", Proceedings of the Institution of Mechanical Engineers, Part G: Journal of Aerospace Engineering 234(11):1788-1810, 2020 (author version).

doi: 10.1177/0954410020919619

Fox, MUST, Prairie Grass, and EMU observations. *Atmos Environ* 2004; 38(28): 4675–4687.

54. Yakhot V, Orszag SA, Thangam S, et al. Development of turbulence models for shear flows by a double expansion technique. *Phys Fluids* 1992; 1510-1520.

55. Jimenez J and Moser R. LES - Where are we and what can we expect. In: *29^{th} AIAA Fluid Dyn Conf*, Albuquerque, USA, 15-18 June 1998.

56. Blazek J. Computational Fluid Dynamics: Principles and Applications. 3^{rd} ed. Butterworth-Heinemann, 2015, pp. 213-252.

57. Pope SB. Ten questions concerning the large-eddy simulation of turbulent flows. *New J Phys* 2004.

58. Sagaut P. Large eddy simulation for incompressible flows. Ed. Springer, 2005.

59. Celik I, Cehreli N and Ibrahim Y. Resolution Quality for Large Eddy Simulations. *J Fluid Eng* 2005; 127.

60. Celik I, Klein M and Janicka J. Assessment measures for engineering LES applications. *J fluids eng* 2009; 131(3).

61. Ivanic T, Foucault E and Pecheux J. Dynamics of swirling jet flows. *Exp Fluids* 2003; 35(4): 317–324.

62. Huang Y, Yang V. Dynamics and stability of lean-premixed swirl-stabilized combustion. *Prog Energy Combust Sci* 2009; 35(4): 293–364.

63. Syred N and Beér JM. Combustion in swirling flows: A review. *Combust Flame* 1974; 23(2): 143–201.

64. Rudgyard M. Integrated preprocessing tools for unstructured parallel cfd applications. Technical report TR/CFD/95/08, CERFACS, 1995.

Payri, R., Novella, R., Carreres, M., Belmar-Gil, M, “Modeling gaseous non-reactive flow in a lean direct injection gas turbine combustor through an advanced mesh control strategy”, Proceedings of the Institution of Mechanical Engineers, Part G: Journal of Aerospace Engineering 234(11):1788-1810, 2020 (author version).

doi: 10.1177/0954410020919619